

# Probing Standard and Non-standard Physics with Ultra-High Energy Neutrinos

By  
Atri Bhattacharya  
PHYS08200704004

Harish-Chandra Research Institute, Allahabad

*A thesis submitted to the  
Board of Studies in Physical Sciences  
In partial fulfilment of requirements  
for the Degree of  
DOCTOR OF PHILOSOPHY  
of  
HOMI BHABHA NATIONAL INSTITUTE*



February, 2014



## **STATEMENT BY AUTHOR**

This dissertation has been submitted in partial fulfillment of requirements for an advanced degree at Homi Bhabha National Institute (HBNI) and is deposited in the Library to be made available to borrowers under rules of the HBNI.

Brief quotations from this dissertation are allowable without special permission, provided that accurate acknowledgement of source is made. Requests for permission for extended quotation from or reproduction of this manuscript in whole or in part may be granted by the Competent Authority of HBNI when in his or her judgment the proposed use of the material is in the interests of scholarship. In all other instances, however, permission must be obtained from the author.

**Atri Bhattacharya**



# DECLARATION

I, hereby declare that the investigation presented in the thesis has been carried out by me. The work is original and has not been submitted earlier as a whole or in part for a degree / diploma at this or any other Institution / University.

**Atri Bhattacharya**



## List of Publications arising from the thesis

### Journal

1. Diffuse Ultra-High Energy Neutrino Fluxes and Physics Beyond the Standard Model,  
Authors: Atri Bhattacharya, Sandhya Choubey, Raj Gandhi and Atsushi Watanabe,  
**Ref: Phys.Lett. B690 (2010) 42-47**
2. Ultra-high neutrino fluxes as a probe for non-standard physics,  
Authors: Atri Bhattacharya, Sandhya Choubey, Raj Gandhi and Atsushi Watanabe,  
**Ref: JCAP 1009 (2010) 009**
3. The Glashow resonance at IceCube: signatures, event rates and  $pp$  vs.  $p\gamma$  interactions,  
Authors: Atri Bhattacharya, Raj Gandhi, Werner Rodejohann and Atsushi Watanabe,  
**Ref: JCAP 1110 (2011) 017**

Atri Bhattacharya



**To my family...**



## Acknowledgments

I would like to thank my supervisor Prof Raj Gandhi who, apart from being a wonderful guide, has also been a pillar of support through my times at HRI. It has been a great pleasure learning from and working with him during this period. I am extremely grateful to my collaborators who have taught me lots. I would especially like to thank Sandhya Choubey, Atsushi Watanabe, Werner Rodejohann, Animesh Chetterjee, Mehedi Masud and Aritra Gupta for all that I have learnt while working with them. Special thanks to Satya, who was for a major duration of my stay at HRI my go-to encyclopaedia for anything Physics. To all the instructors at HRI whose courses taught me so much, I extend my deepest gratitude.

To friends at HRI who have always been there for me, through my thick and thin, there is nothing I can say here that will express my gratitude enough. Nonetheless, it would be remiss not to mention Arjun Bagchi, Turbasu Biswas, Shamik Banerjee, Sanjoy Biswas, Joydeep Chakroborty, Satyanarayan Mukhopadhyay, Sourav Mitra, Sourabh Niyogi, Ujjal Dey, Saurabh Pradhan, Sabyasachi and Paromita Tarat, Manoj Mandal, Anirban Basu, Animesh “God” Chetterjee, Shankha Banerjee, Mehedi Masud, Shrobona Bagchi, Nyayabanta Swain, Raghunath Ghara, Dharmadas Jash, Abhishek Chowdhury, Anushree Ghosh, Taushif Ahmed, Narayan Rana, Aritra Gupta, Dibya Kanti Mukherjee, Sauri Bhattacharya, Nabarun Chakrabarty, Tomoghna Das, Arijit Dutta, Samrat Kadge, Titas Chanda and Dipyaman Pramanik, without each of whom I would probably not have been able to put up with six years of life at HRI.

I would like to thank my parents and my brother who have all been thoroughly encouraging and uplifting for as long as I can remember.

Lastly, I would like to thank Ipsita for not only putting up with me during this period, but also for agreeing to do so for life, and for always being supportive and motivating whenever I needed a pillar of strength.



# Contents

<b>SYNOPSIS</b>	<b>xv</b>
<b>List of Figures</b>	<b>xvii</b>
<b>List of Tables</b>	<b>xix</b>
<b>I Introduction</b>	<b>1</b>
<b>1 Ultra-high energy neutrinos and extra-galactic sources</b>	<b>3</b>
1.1 Neutrinos at the highest energies . . . . .	3
1.2 Ultra-high energy neutrino fluxes . . . . .	6
1.3 Example of an extra-galactic source: Active Galactic Nuclei . . . . .	7
<b>II Glashow Resonance - The Highest Energy Standard Model Interaction</b>	<b>11</b>
<b>2 The Glashow Resonance as a pointer to physics at extra-galactic sources</b>	<b>13</b>
2.1 Introduction to the Glashow Resonance process . . . . .	13
2.2 The Glashow-resonance and its relevance to present day UHE neutrino detection . . . . .	14
<b>3 Event rates and signal/background ratio from the GR process</b>	<b>17</b>
3.1 Shower signatures of the Glashow resonance . . . . .	17
3.2 Novel signatures of the Glashow resonance . . . . .	21
3.3 Conclusion . . . . .	25

<b>III</b>	<b>Probing Non-Standard Physics with Events at IceCube</b>	<b>27</b>
<b>4</b>	<b>Introduction</b>	<b>29</b>
4.1	Spectral Averaging due to Oscillations . . . . .	29
<b>5</b>	<b>Effect of Non-Standard Physics on Neutrino Propagation</b>	<b>31</b>
5.1	Effect of neutrino decay . . . . .	32
5.1.1	Introduction to neutrino decay . . . . .	32
5.1.2	Effect of neutrino decay on the flavour fluxes . . . . .	33
5.1.3	Modification of total UHE events due to decay . . . . .	37
5.2	Effect of non-zero CP violating phase and $\theta_{13}$ variation on neutrino decay .	39
5.2.1	Variation of $\theta_{13}$ . . . . .	41
5.2.2	Non-zero CP violating phase. . . . .	41
5.3	Effect of Lorentz symmetry violation . . . . .	43
5.3.1	Modification of neutrino transition probabilities due to LV effects .	44
5.3.2	Effect of Lorentz violation on neutrino flavour fluxes . . . . .	44
5.3.3	Detectability of Lorentz-violation . . . . .	46
5.4	Pseudo-Dirac neutrinos . . . . .	46
5.5	Effect of decoherence during neutrino propagation . . . . .	47
<b>IV</b>	<b>Conclusion</b>	<b>51</b>
	<b>Bibliography</b>	<b>55</b>

# SYNOPSIS

During my doctorate work, I have studied various aspects of neutrinos at extremely high energies ( $> 10$  TeV), specifically with a view to unravelling possible hints of non-standard physics that might be embedded in such events. Neutrinos at energies greater than 10 TeV are produced in the extremely energetic cores and jets of astrophysical sources located either within our galaxy (*e.g.* pulsars, supernovae, etc.) or outside our galaxy (*e.g.* active galactic nuclei (AGN), gamma ray bursts (GRB), etc.). Thereafter, being extremely inert, they stream to the earth almost unperturbed, with only oscillation among the three flavours modifying their fluxes. Because the fluxes of the neutrinos produced at these energies are extremely low, detecting them at the earth requires detectors with very large volumes ( $\sim \text{Km}^3$ ). The IceCube (IC), built at the South Pole into the Antarctic ice bed, is a  $1 \text{ Km}^3$  detector designed to detect and study such high energy neutrinos. My work has involved analysing the neutrino events that might be seen at IC, in the future, to understand *a)* the nature of the source producing these neutrinos, *b)* the nature of mixing among the three flavours as the neutrinos oscillate while propagating from the source to the earth, specifically looking at whether it is in keeping with standard physics or affected by small non-standard physical effects such as neutrino decay, violation of Lorentz invariance, etc., and *c)* novel signatures of the highest energy standard model process hitherto unseen, *viz.* the Glashow Resonance (GR),

$$\bar{\nu}_e + e^- \rightarrow W^- ,$$

occurring when a  $\bar{\nu}_e$  with energy of 6.3 PeV (in the lab frame) interacts with an electron within the IceCube resulting in the production of  $W^-$  at resonance, which then decays promptly into hadrons and, to about one-sixth of the time, into leptons.

IceCube is capable of distinguishing between the three flavours of neutrinos, as they interact with the nuclei within the detector, by means of their event topologies: *a)* showers due to charged current interactions of the  $\nu_e$  and, for incident energies less than a PeV,  $\nu_\tau$ , and, neutral current interactions of all the three flavours, *b)* muon-track events due to the charged current interactions of  $\nu_\mu$ , and finally *c)* signature topologies of the  $\nu_\tau$  at energies above a PeV, such as the double bang, lollipop, etc. In my work with my supervisor and

other collaborators, we have shown that, as IceCube collects a significant number of events over the next five years, it will be possible, by comparing the fluxes of three flavours, to detect signatures of non-standard physics, if any, on the neutrino oscillation probabilities at these energies. By considering each of neutrino decay, Lorentz violation, existence of additional pseudo-Dirac neutrinos and quantum decoherence in turn, we have predicted the expected parameter space in each case that such high energy events will be sensitive to, and should therefore be able to rule out if the events are consistent with expectation from standard physics.

Finally, we have also discussed the possibility of seeing the GR in the IceCube. Specifically we have calculated the expected number of shower events around the GR energies, *i.e.*  $\sim 6.3$  PeV as a function of the source spectrum and discuss the rare but tell-tale and completely background-free events seen when the resonantly produced W decays to leptons, rather than to hadrons. We have also shown how non-standard physical effects might modify the number of events otherwise expected around the GR energies.

# List of Figures

1.1	The neutrino sky – Energies across which neutrinos are produced in the universe . . . . .	5
1.2	Experimental bounds on astrophysical diffuse neutrino flux . . . . .	10
2.1	Pure muon . . . . .	15
2.2	Contained lollipop . . . . .	15
3.1	Shwer spectrum from a pure $pp$ source . . . . .	18
3.2	Shower spectrum from a pure $p\gamma$ source . . . . .	19
3.3	Ratio of resonant to off-resonant events as a function of $x$ . . . . .	20
3.4	Event spectrum for pure muon events; $pp$ source . . . . .	22
3.5	Event spectrum for contained lollipops; $pp$ source . . . . .	23
3.6	Estimate for total events from Glashow Resonance against $x$ . . . . .	24
4.1	Flavour mixing due to neutrino oscillation . . . . .	30
5.1	Fluxes modified due to incomplete decay . . . . .	35
5.2	Effect of lifetime variation on fluxes post incomplete decay . . . . .	36
5.3	Ratio of track to shower events post decay . . . . .	40
5.4	Effect of $\theta_{13}$ variation on post-decay fluxes . . . . .	41
5.5	Effect of $\delta_{CP}$ variation on post-decay fluxes, normal hierarchy . . . . .	42
5.6	Effect of $\delta_{CP}$ variation on post-decay fluxes, both hierarchies . . . . .	43
5.7	Effect of Lorentz violation for varying parameter strengths . . . . .	45
5.8	Effect of existence of pseudo-Dirac species . . . . .	48
5.9	Effect of decoherence . . . . .	49



# List of Tables

- 2.1 Cross-sections for electron anti-neutrino interactions at  $E = 6.3$  PeV. . . . 15
- 2.2 Cross-sections for non-resonant interactions at  $E = 6.3$  PeV. . . . . 16
- 3.1 Estimated event-rates at IceCube . . . . . 25
- 5.1 Estimate of decay-modified shower and muon track event-rates . . . . . 39



# Part I

## Introduction



# Chapter 1

## Ultra-high energy neutrinos and extra-galactic sources

### 1.1 Neutrinos at the highest energies

The neutrino sky spans about twenty five orders of magnitude in energy, potentially offering the possibility of probing the universe at widely disparate energy scales. The vast range of energies across which neutrinos are expected to be seen at terrestrial detectors is shown in Fig. 1.1 – it ranges from relic neutrinos with microwave energies ( $10^{-6}$  eV) produced in the very early universe to cosmogenic neutrinos produced due to the interaction of cosmic ray protons with the cosmic microwave background photons and having energies as high as  $10^{20}$  eV. It should be stressed here that Fig. 1.1 represents a combination of observations and theoretical predictions. In particular, neutrinos at the highest energies, including above the tens of *TeV*, have not yet been detected. The dominant sources of neutrinos at the different energies include

1. Relic neutrinos, remnants from a very early universe, set the lowest boundary of the spectrum with energies  $\sim 10^{-6}$  eV,
2. Solar neutrinos have already been detected at the keV and MeV energies [1],
3. Neutrinos from supernovae bursts such as those seen from the SN1987A [2], and those produced at earth in reactors populate the MeV to low GeV energies,
4. Atmospheric neutrinos, produced when cosmic rays interact with the nuclei in the earth's atmosphere, populate a large range of energies themselves, having been detected with energies from tens of MeV's upto a few GeV's and are expected to have significant fluxes up to the low TeV's (See [3] for a detailed review),

5. The higher end of the spectrum beyond the TeV energies and extending upto the EeV energies includes neutrinos predominantly expected from high energy photo-hadronic interactions at extra-galactic sources, and which have not yet been detected. These include
  - Neutrinos from photo-hadronic sources such as Active Galactic Nuclei and Gamma-Ray Bursts producing neutrinos predominantly at energies from a few TeV's upto tens of PeV's ( $10^6$  GeV), and
  - At the very edge of the high energy spectrum neutrinos produced by the cosmogenic interaction where protons from cosmic rays interact with the CMB photons to produce mesons that decay to neutrinos at  $10^{18}$

In addition to being seen across such diverse energies, the neutrinos also have the property of essentially free-streaming to the earth once produced at the source, only being modified by oscillation among the three flavours while being relatively inert to interactions with any other standard model (SM) particle species. Indeed neutrinos, because they interact only via the weak interaction, have the least interaction strengths among all the SM particles. Consequently, when neutrinos are detected as coming from a particular astrophysical source, they can serve as obvious pointers to the nature of physics responsible for their production within the source itself.

As noted above, the high end ( $10^{11} - 10^{12}$  GeV) of this remarkably broad band in energy is set by: a) GZK neutrinos [4, 5], which originate in the interactions of the highest energy cosmic rays with the cosmic microwave photon background and b) neutrinos from the most energetic astrophysical objects observed in the universe, *i.e.* active galactic nuclei (AGNs) and Gamma-Ray bursts (GRBs). Detection, still in the future, presents both considerable opportunities and formidable challenges. In particular, at the ultra-high energies ( $10^5$  GeV and above) which will be the focus of this thesis, the tiny fluxes that arrive at earth require detectors that combine the capability to monitor very large detection volumes with innovative techniques (for reviews, see e.g. [6] and [7]). Examples of such detectors are AMANDA [23], ICECUBE [9], BAIKAL [10], ANTARES [11], RICE [12] and ANITA [13].

A compelling motivation for exploring UHE neutrino astronomy is the fact that the origin of cosmic rays (CR) beyond the “knee” ( $10^6$  GeV) remains a mystery many decades after their discovery. Additionally, CR with energies in excess of  $10^{11}$  GeV have been observed [14, 15], signalling the presence of astrophysical particle accelerators of unprecedentedly high energies. If protons as well as neutrons are accelerated at these sites in addition to electrons, standard particle physics predicts correlated fluxes of neutrons and neutrinos which escape from the confining magnetic field of the source, while protons and electrons stay trapped. Generically, the electrons lose energy rapidly via synchrotron radiation. These radiated photons provide a target for the accelerated protons, which results in the production of pions, muons and ultimately, neutrinos in the ratio

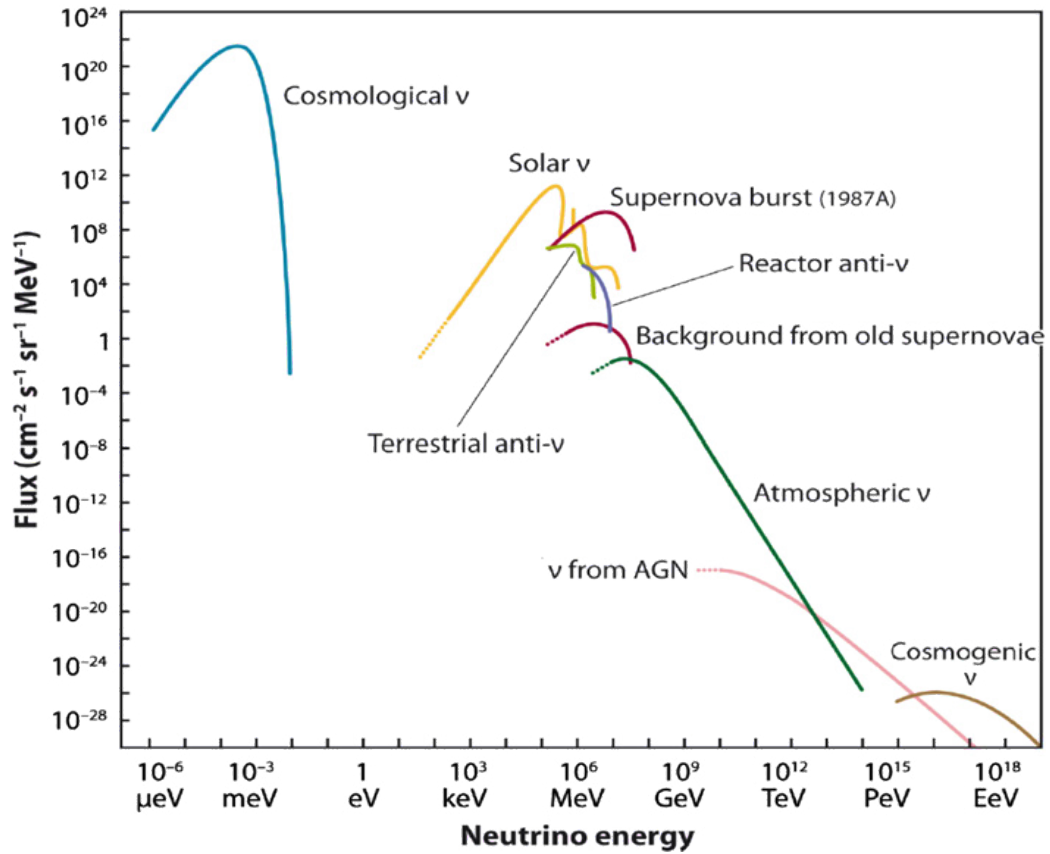


Figure 1.1: The vast expanse of energies across which neutrinos are produced in the universe at different sources, which thereafter stream freely to the earth affected largely only by oscillation among the three flavours.

$\nu_e : \nu_\mu : \nu_\tau = 1 : 2 : 0$ . The detection and study of ultra-high energy (UHE) neutrinos is thus a probe of the origin of CR and the physics of UHE astrophysical accelerators.

## 1.2 Ultra-high energy neutrino fluxes

The search for cosmic neutrinos with PeV energies is motivated by observations of cosmic rays. It has been conjectured that cosmic ray engines accelerate protons and confine them with magnetic fields in the acceleration region. The accelerated protons interact with ambient photons or protons, producing neutrons and charged pions. Charged particles are trapped by magnetic fields, while neutral particles escape from the source region, decay and produce observable cosmic rays and neutrinos. If the source region is optically thin, the energy density of neutrinos scales linearly with the cosmic ray density and the neutrino intensities are co-related with the observed cosmic ray flux.

The result of these considerations for the expected total neutrino flux (the sum over all species) at the source is set by the Waxman-Bahcall flux, given by [139]

$$E_\nu^2 \Phi_{\nu+\bar{\nu}} = 2 \times 10^{-8} \epsilon_\pi \xi_z \quad (\text{GeV cm}^{-2} \text{ s}^{-1} \text{ sr}^{-1}). \quad (1.1)$$

Here  $\xi_z$  is a function of the red-shift parameter  $z$  alone, representing the evolution of sources with red-shift, and  $\epsilon_\pi$  is the ratio of pion energy to the emerging nucleon energy at the source. One has  $\xi_z \approx 0.6$  for no source evolution, while  $\xi_z \approx 3$  for an evolution  $\propto (1+z)^3$ . Depending on the relative ambient gas and photon densities, the neutrino production originates in either  $p\gamma$  or  $pp$  interactions. For the  $pp$  case  $\epsilon_\pi \approx 0.6$  and for the  $p\gamma$  case  $\epsilon_\pi \approx 0.25$ .

Since source distributions and types are not well known, we parameterize the relative  $pp$  and  $p\gamma$  contributions to the total flux with a dimensionless parameter  $x$ ,  $0 \leq x \leq 1$ , so that

$$\Phi_{\text{source}} = x \Phi_{\text{source}}^{pp} + (1-x) \Phi_{\text{source}}^{p\gamma}, \quad (1.2)$$

where  $\Phi^{pp/p\gamma}$  represents the neutrino flux from  $pp/p\gamma$  interactions. We assume here that neutron decays, which (as discussed in [137]) could be present in certain sources give negligible contributions to the overall flux. Effects like multi-pion processes producing  $\pi^-$  events in  $p\gamma$  sources, can be included in the parameterization.

The flavor composition at the source is given by  $(\nu_e, \nu_\mu, \nu_\tau) = (\bar{\nu}_e, \bar{\nu}_\mu, \bar{\nu}_\tau) \approx (1, 2, 0)$  for a  $pp$  source and  $(\nu_e, \nu_\mu, \nu_\tau) \approx (1, 1, 0)$  and  $(\bar{\nu}_e, \bar{\nu}_\mu, \bar{\nu}_\tau) \approx (0, 1, 0)$  for the  $p\gamma$  case. These configurations are changed by the incoherent propagation from the source to earth. The transition probabilities between flavor eigenstates are described by three mixing angles and one CP violating phase. By using  $\theta_{12} = 35^\circ$ ,  $\theta_{13} = 0$ , and  $\theta_{23} = 45^\circ$  as reference values of the lepton mixing angles, the flavor ratios at the earth become  $(\nu_e, \nu_\mu, \nu_\tau) = (\bar{\nu}_e, \bar{\nu}_\mu, \bar{\nu}_\tau) =$

(1, 1, 1) for  $pp$ , while  $(\nu_e, \nu_\mu, \nu_\tau) = (0.78, 0.61, 0.61)$  and  $(\bar{\nu}_e, \bar{\nu}_\mu, \bar{\nu}_\tau) = (0.22, 0.39, 0.39)$  for fluxes from  $p\gamma$  interactions. Finally, the flux for each neutrino species is given by

$$E_\nu^2 \Phi_{\nu_e} = 2 \times 10^{-8} \xi_z \left[ x \frac{1}{6} \cdot 0.6 + (1-x) \frac{0.78}{3} \cdot 0.25 \right], \quad (1.3)$$

$$E_\nu^2 \Phi_{\nu_\mu} = 2 \times 10^{-8} \xi_z \left[ x \frac{1}{6} \cdot 0.6 + (1-x) \frac{0.61}{3} \cdot 0.25 \right] = E_\nu^2 \Phi_{\nu_\tau}, \quad (1.4)$$

$$E_\nu^2 \Phi_{\bar{\nu}_e} = 2 \times 10^{-8} \xi_z \left[ x \frac{1}{6} \cdot 0.6 + (1-x) \frac{0.22}{3} \cdot 0.25 \right], \quad (1.5)$$

$$E_\nu^2 \Phi_{\bar{\nu}_\mu} = 2 \times 10^{-8} \xi_z \left[ x \frac{1}{6} \cdot 0.6 + (1-x) \frac{0.39}{3} \cdot 0.25 \right] = E_\nu^2 \Phi_{\bar{\nu}_\tau}, \quad (1.6)$$

in units of  $\text{GeV cm}^{-2} \text{s}^{-1} \text{sr}^{-1}$ . The equalities between  $\nu_\mu$  and  $\nu_\tau$  flavors, both for neutrinos and anti-neutrinos, are the consequence of vanishing  $\theta_{13}$  (actually, vanishing of the real part of  $U_{e3}$  would suffice) and maximal  $\theta_{23}$  used in the calculation. The uncertainty in  $\theta_{13}$  and  $\theta_{23}$  breaks this equality and changes each flux by at most 10%. Note that the total intensity becomes maximal for the pure  $pp$  case  $x = 1$ . With a strong evolution value  $\xi_z = 3$ , the maximal value is  $\sum_\alpha E_\nu^2 \Phi_{\nu_\alpha + \bar{\nu}_\alpha} = 3.6 \times 10^{-8} \text{GeV cm}^{-2} \text{s}^{-1} \text{sr}^{-1}$ , which agrees with the latest upper bound on the  $E^{-2}$  spectrum [140].

Unless otherwise mentioned, we use these fluxes with  $\xi_z = 3$  as an example to calculate the event rates.

### 1.3 Example of an extra-galactic source: Active Galactic Nuclei

Active galactic nuclei are extremely distant galactic cores having very high densities and temperatures. Due to the high temperatures and the presence of strong electromagnetic fields, AGN's act as accelerators of fundamental particles, driving them to ultra-high energies ( $> 1000$  GeV). The acceleration of electrons as well as protons (or ions) by strong magnetic fields in cosmic accelerators like AGN's leads to neutrino production. Specifically, accelerated electrons lose their energy via synchrotron radiation in the magnetic field leading to emission of photons that act as targets for the accelerated protons to undergo photo-hadronic interactions. This leads to the production of mesons which are unstable and decay. In the standard case the charged pions decay primarily contributing to neutrino production via  $\pi^\pm \rightarrow \mu^\pm \nu_\mu$  and subsequent muon decay via  $\mu^\pm \rightarrow e^\pm \nu_\mu \nu_e$ . This leads to a flavour flux ratio of  $(\nu_e : \nu_\mu : \nu_\tau) = 1 : 2 : 0$  in the standard case. The particles finally produced as a result of this process are, thus, high energy neutrons, photons, electron pairs and neutrinos.

In this section we calculate the diffuse flux spectrum of neutrinos escaping from both

optically thick AGN's, which are so called because they are opaque to neutrons and trap them, and optically thin AGN's, which are neutron-transparent, and detected at distant detectors, for instance, at IceCube [23].

To calculate the flux from optically thick sources, we use the spectra of neutrinos produced in a standard AGN source, as discussed in detail in [86]. We then account for red-shifting in the energy dependence of the spectra appropriately. To obtain the upper bound for the diffuse AGN flux we vary the break energy  $E_b$  within the allowed range and maximally superpose all the resulting spectra. To obtain the diffuse AGN flux spectrum at earth using a standard AGN distribution across the universe, we integrate the red-shifted spectra from the individual sources over the standard AGN distribution in the universe. The resulting diffuse bound and spectrum are then normalised using the cosmic ray bounds also obtainable using a similar calculation for the cosmic ray spectrum, but here used directly from [86].

Following [86], we assume that the production spectra for neutrons and cosmic rays from a single AGN are given by

$$Q_n(E_n, L_p) \propto L_p \exp \left[ \frac{-E_n}{E_{\max}} \right] \begin{cases} E_n^{-1} E_b^{-1} & (E_n < E_b) \\ E_n^{-2} & (E_b < E_n) \end{cases}, \quad (1.7)$$

$$Q_{\text{cr}}(E_p, L_p) \propto L_p \exp \left[ \frac{-E_p}{E_{\max}} \right] \begin{cases} E_p^{-1} E_b^{-1} & (E_p < E_b) \\ E_p^{-3} E_b & (E_b < E_p) \end{cases}, \quad (1.8)$$

where

- $Q_n$  and  $Q_{\text{cr}}$  represent the neutron and cosmic ray spectrum respectively, as a function of the neutron and proton energies  $E_n$  and  $E_p$  respectively,
- $L_p$  represents the proton luminosity of the source,
- $E_b$  is the spectrum breaking energy which can vary from  $10^7$  GeV to  $10^{10}$  GeV for optically thick AGN sources, and finally,
- $E_{\max}$  is the cutoff energy beyond which the spectra fall off steeply.

Using Eq. (1.7) the generic neutrino production spectrum from AGN's can be written as

$$Q_{\nu_\mu}(E) \approx 83.3 Q_n(25E) \quad (1.9)$$

We now need to account for red-shifting in the energies of the neutrinos propagating over cosmological distances prior to arriving at the detector. It is convenient to describe the red-shifting in terms of the dimensionless red-shift parameter  $z$ , defined as

$$\frac{\lambda}{\lambda_0} = 1 + z,$$

$\lambda$  and  $\lambda_0$  being wavelengths of a propagating signal at detector and at source respectively. In terms of  $z$  the energy of a particle at source ( $E_0$ ) and at the detector ( $E$ ) can be related via

$$\frac{E_0}{E} = 1 + z.$$

Thus, to account for red-shifting in the energy of the neutrinos we replace the source energy  $E$  in Eq. (1.9) by  $E(1+z)$ . We now incorporate standard neutrino oscillations by multiplying the spectrum with the oscillation probabilities. The probability of a neutrino flavour  $\nu_\alpha$  oscillating to another  $\nu_\beta$  is given by

$$P_{\alpha \rightarrow \beta} = \delta_{\alpha\beta} - 4 \sum_{i>j} \mathcal{R}e (U_{\alpha i}^* U_{\beta i} U_{\alpha j} U_{\beta j}^*) \sin^2 \left( \frac{\Delta m_{ij}^2 L}{4E} \right) \quad (1.10)$$

However, as the distances involved are very large, oscillation only provides a  $z$ -independent averaging effect over the three flavours. In all our calculations, unless otherwise mentioned, the CP violating phase  $\delta_{CP}$  is kept 0 and the  $3\sigma$  best-fit values of the mixing angles [87] are used, i.e.,

$$\sin^2(\theta_{12}) = 0.321, \quad \sin^2(\theta_{23}) = 0.47, \quad \sin^2(\theta_{13}) = 0.003.$$

The intensity at earth for an input spectrum  $Q[(1+z)E, z]$  is given by

$$I(E) \propto \int_{z_{\min}}^{z_{\max}} \frac{(1+z)^2}{4\pi d_L^2} \frac{dV_c}{dz} \frac{dP_{\text{gal}}}{dV_c} Q[(1+z)E, z] dz \quad (1.11)$$

with  $d_L$  and  $V_c$  representing the luminosity distance and co-moving volume respectively.

To obtain the maximal bound for the diffuse flux from the optically thick sources we start with  $E_b = 10^7$  GeV in the input spectrum  $Q$  and carry out the above integration using  $z_{\min} = 0.03$  and  $z_{\max} = 6$ . The value of  $E_b$  is varied from  $10^7$  GeV to  $10^{10}$  GeV and the above integration is carried out for each case. The resulting  $I_{E_b}(E)$  are then superposed to obtain the final bound. This is then normalised using the observed cosmic ray spectrum to give the upper bound of the diffuse flux for the three neutrino flavours at the detector. As may be expected, it leads to a result similar to that obtained in [86], with, however, the results of standard oscillations incorporated. A related procedure is used for calculating the fluxes from optically-thin sources. We call this normalised upper bound of diffuse fluxes the *MPR bound*, and use this as the reference flux for all our calculations. The MPR bound is a modification of the Waxman-Bahcall (W & B) bound [85], where a uniform  $E^{-2}$  input spectrum of extragalactic cosmic rays was used to calculate the diffuse fluxes. This difference is noticeable in, *e.g.*, Fig. 5.1 where we have shown both these reference bounds. The resultant MPR bounds for both types of sources are shown in all

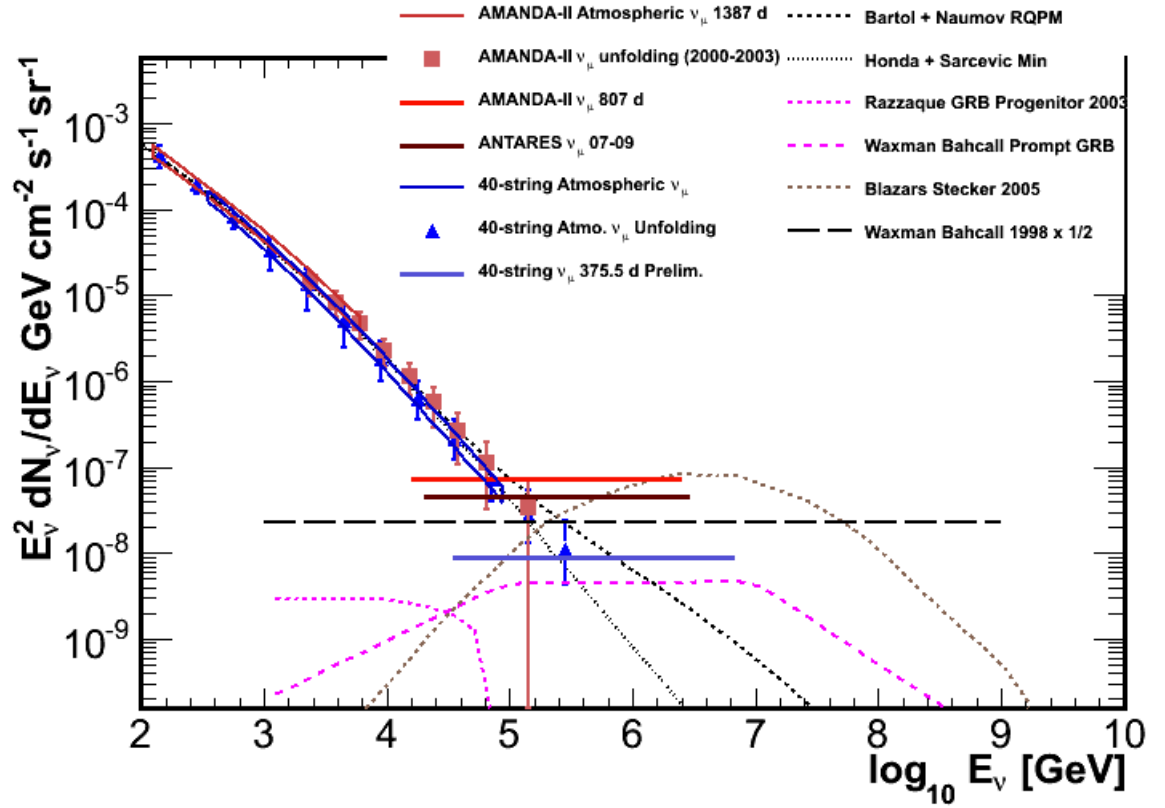


Figure 1.2: Present experimental bounds from IceCube on the diffuse  $\nu_\mu$  flux assuming an  $E^{-2}$  injection spectrum at source [140]. Predictions of neutrino fluxes from several theoretical models are also shown.

the figures as unbroken gray lines.

## Part II

# Glashow Resonance - The Highest Energy Standard Model Interaction



# Chapter 2

## The Glashow Resonance as a pointer to physics at extra-galactic sources

### 2.1 Introduction to the Glashow Resonance process

Since the ultra-high energy neutrinos span a wide range of energies, they can be sensitive to the Glashow Resonance (GR) [132], which refers to the resonant formation of an intermediate  $W^-$  in  $\bar{\nu}_e e$  collision at the anti-neutrino energy  $E_{\bar{\nu}} = 6.3 \text{ PeV} \simeq 10^{6.8} \text{ GeV}$ . This is a particularly interesting process [135, 136, 137, 138], unique in its sensitivity to only anti-neutrinos. In particular, because the relative  $\bar{\nu}_e$  content of  $pp$  and  $p\gamma$  collision final states is very different, the question of which of these two processes lie at the origin of high energy neutrinos can, in principle, be tested well with GR events. Indeed, earlier works have focused mainly on the resonance detection via shower events and on how the GR can be used as a discriminator of the relative abundance of the  $pp$  and  $p\gamma$  sources.

The significance of the GR is not simply limited to the detectability of the resonance process itself, but also pertains to its feasibility as a tool to detect the first extra-galactic diffuse neutrino signals themselves. We recalculate expected GR event numbers and their dependence on the relative contribution of  $pp$  and  $p\gamma$  sources. Our work updates and generalizes the results of [135]. To calculate the number of events, we use the Waxman–Bahcall  $E^{-2}$  spectrum [139] as a benchmark neutrino spectrum. The current limits on the neutrino flux have been shown previously in Fig. 1.2.

If the neutrino flux is to be observed, it will emerge above the atmospheric background while staying below the current experimental upper bounds. The present status of these limits leads us to believe that this is likely to happen at energies of  $10^6 \text{ GeV}$  or greater, close to region of the Glashow resonance. Therefore, it is useful and timely to re-examine this resonance region carefully to reassess its potential as a tool to detect the cosmic diffuse neutrinos.

We point out that there are two types of distinctive resonant processes besides the standard shower signatures from  $\bar{\nu}_e e \rightarrow \text{hadrons}$  and  $\bar{\nu}_e e \rightarrow \bar{\nu}_e e$  considered in the literature. We call these new signatures “pure muon” and “contained lollipop” events. A pure muon event occurs when only a muon track (and nothing else) is created inside the detector volume by the resonant process  $\bar{\nu}_e e \rightarrow \bar{\nu}_\mu \mu$ . We sketch the signature in Fig. 2.1. Unlike the neutrino–nucleon charged current scattering  $\nu_\mu N \rightarrow \mu X$  (and its charge conjugated counterpart), the pure muon track is not accompanied by any shower activity at its starting point. We note that in  $\nu_\mu N \rightarrow \mu X$  processes with PeV neutrino energies, about 26% of the initial neutrino energy is transferred to the kicked quark, which turns into a hadronic cascade [141]. Thus, a muon track from  $\nu_\mu N \rightarrow \mu X$  is accompanied by a  $\sim 200$  m radius shower at the interaction vertex for PeV neutrino energies. This is clearly distinguishable from the muons of the pure muon event  $\bar{\nu}_e e \rightarrow \bar{\nu}_\mu \mu$ . A possible background against this signal is the non-resonant electroweak process  $\nu_\mu e \rightarrow \mu \nu_e$ . The cross section is however three orders of magnitude smaller than  $\bar{\nu}_e e \rightarrow \bar{\nu}_\mu \mu$  at the resonant energy. The pure muon is therefore essentially background free in the neighborhood of the resonance energy and even one event implies discovery of the resonance and signals the presence of diffuse extra-galactic flux.

A contained lollipop event occurs for  $\bar{\nu}_e e \rightarrow \bar{\nu}_\tau \tau$ : a tau is created and decays inside the detector with a sufficient length of the tau track, see Fig. 2.2. Again, due to the lack of shower activity at the initial vertex, the contained lollipop is also clearly separated from the standard double bang [142] signature induced by the  $\nu_\tau N + \bar{\nu}_\tau N$  charged current scattering, and it is therefore also essentially free from background.

## 2.2 The Glashow-resonance and its relevance to present day UHE neutrino detection

Ultra-high energy electron anti-neutrinos allow the resonant formation of  $W^-$  in their interactions with electrons, at 6.3 PeV. This process, known as the Glashow resonance [132, 133, 134] has, in the resonance energy band, several notably high cross-sections for the allowed decay channels of the  $W^-$ . In particular, the differential cross-section for  $\bar{\nu}_e e \rightarrow \bar{\nu}_\mu \mu$  is given by

$$\frac{d\sigma}{dy} (\bar{\nu}_e e \rightarrow \bar{\nu}_\mu \mu) = \frac{G_F^2 m E_\nu}{2\pi} \frac{4(1-y)^2 (1 - (\mu^2 - m^2)/2mE_\nu)^2}{(1 - 2mE_\nu/M_W^2)^2 + \Gamma_W^2/M_W^2}, \quad (2.1)$$

and, for hadrons one may write

$$\frac{d\sigma}{dy} (\bar{\nu}_e e \rightarrow \text{hadrons}) = \frac{d\sigma}{dy} (\bar{\nu}_e e \rightarrow \bar{\nu}_\mu) \times \frac{\Gamma(W \rightarrow \text{hadrons})}{\Gamma(W \rightarrow \bar{\nu}_\mu \mu)}. \quad (2.2)$$

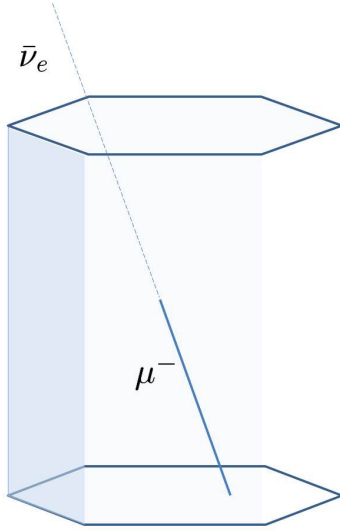


Figure 2.1: Pure muon

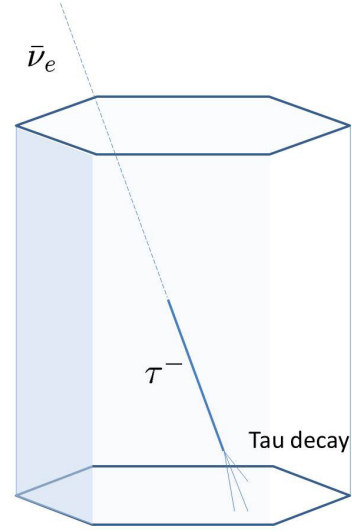


Figure 2.2: Contained lollipop

The above expressions hold in the lab frame where  $m =$  electron mass,  $\mu =$  muon mass,  $M_W = W^-$  mass,  $y = E_\mu/E_\gamma$ , and  $\Gamma_W$  is the total width of the  $W$ .

Table 2.1 [141] lists the total cross-sections at  $E_\nu^{\text{res}} = 6.3$  PeV. We note that for the leptonic final states, one expects (very nearly) equal cross-sections regardless of whether one produces  $\bar{\nu}_\mu\mu$ ,  $\bar{\nu}_\tau\tau$  or  $\bar{\nu}_ee$ .

Interaction	$\sigma[\text{cm}^2]$
$\bar{\nu}_ee \rightarrow \bar{\nu}_ee$	$5.38 \times 10^{-32}$
$\bar{\nu}_ee \rightarrow \bar{\nu}_\mu\mu$	$5.38 \times 10^{-32}$
$\bar{\nu}_ee \rightarrow \bar{\nu}_\tau\tau$	$5.38 \times 10^{-32}$
$\bar{\nu}_ee \rightarrow \text{hadrons}$	$3.41 \times 10^{-31}$
$\bar{\nu}_ee \rightarrow \text{anything}$	$5.02 \times 10^{-31}$

Table 2.1: Cross-sections for electron anti-neutrino interactions at  $E = 6.3$  PeV.

In Table 2.2 we list, also at  $E_\nu = 6.3$  PeV, the possible non-resonant interactions which could provide backgrounds to the interactions listed in Table 2.1. We note that the total resonant cross-section,  $\bar{\nu}_ee \rightarrow \text{anything}$  is about 360 times higher than the total neutrino-nucleon cross-section,  $\nu_\mu N \rightarrow \mu + \text{anything}$ . The cross-section for  $\bar{\nu}_ee \rightarrow \text{hadrons}$  is about 240 times its non-resonant hadron producing background interaction  $\nu_\mu N \rightarrow \mu + \text{anything}$ . Even the resonant leptonic final state interactions have cross-sections about 40 times that of the total  $\nu_\mu N \rightarrow \mu + \text{anything}$  cross-section. Finally we

Interaction	$\sigma[cm^2]$
$\nu_\mu N \rightarrow \mu + \text{anything}$	$1.43 \times 10^{-33}$
$\nu_\mu N \rightarrow \nu_\mu + \text{anything}$	$6.04 \times 10^{-34}$
$\nu_\mu e \rightarrow \nu_e \mu$	$5.42 \times 10^{-35}$

Table 2.2: Cross-sections for non-resonant interactions at  $E = 6.3$  PeV.

note that the “pure-muon” and “contained lollipop” resonant processes discussed in the Sec. 2.1 have negligible backgrounds. For example, the process  $\bar{\nu}_e e \rightarrow \bar{\nu}_\mu \mu$  (pure muon) has a cross-section about 1000 times higher than its non-resonant counterpart  $\nu_\mu e \rightarrow \nu_e \mu$ .

Given the considerations and the fact that the present bounds shown in Fig. 1.2 restrict observational diffuse fluxes to energies above  $10^6$  GeV (*i.e.*, close to the GR region), the GR, inspite of its narrow span of energy, may be an important discovery tool for the yet to be observed extra-galactic diffuse neutrino spectrum.

# Chapter 3

## Event rates and signal/background ratio from the GR process

As discussed before, we will look at both shower and muon/tau-track events to identify unique signatures for cosmic neutrinos via the Glashow resonance. In this context, we first focus on the shower events.

### 3.1 Shower signatures of the Glashow resonance

Among the resonance processes, it turns out that the only channel significantly contributing to the events is the hadronic interaction  $\bar{\nu}_e e \rightarrow \text{hadrons}$ , while the contributions from the other channels are negligibly small. Beside the hadronic channel, the following two decay modes produce electromagnetic showers in the detector; *i*)  $\bar{\nu}_e e \rightarrow \bar{\nu}_e e$  and *ii*)  $\bar{\nu}_e e \rightarrow \bar{\nu}_\tau \tau$  with  $E_\tau \lesssim 2 \text{ PeV}$ . A tau of  $E_\tau \gtrsim 2 \text{ PeV}$  travels more than 100 m before decay and can be separated from a single shower<sup>1</sup>. Notice that the hadronic channel constitutes 68% of the total decay width of  $W^-$ , whereas *i*) and *ii*) constitute 11% each. Furthermore, only half of the parent neutrino energy becomes shower energy in *i*) and *ii*), while all energy is converted to shower energy in the hadronic mode.

The event rate of  $\bar{\nu}_e e \rightarrow \text{hadrons}$  is calculated as

$$\text{Rate} = 2\pi \frac{10}{18} N_A V_{\text{eff}} \int dE_\nu \int_0^1 dy \frac{d\sigma}{dy} \Phi_{\bar{\nu}_e}(E_\nu), \quad (3.1)$$

where  $N_A = 6.022 \times 10^{23} \text{ cm}^{-3}$  and  $V_{\text{eff}} \approx 2 \text{ km}^3$ , and  $d\sigma/dy$  is the neutrino–electron cross section [141]. The effective volume is taken as twice as large as the instrumental volume since the radius of the showers with the resonant energy is about 300 m. The events are

---

<sup>1</sup>This is identified as the contained lollipop if the shower provided by the tau decay occurs inside the detector volume.

integrated over the upper half sphere since up-moving electron neutrinos are attenuated by the earth matter. At the resonance peak, the integrated cross section is  $3.4 \times 10^{-31} \text{ cm}^2$ . With the  $pp$  ( $p\gamma$ ) source flux  $E_\nu^2 \Phi_{\bar{\nu}_e} = 6$  ( $1.1$ )  $\times 10^{-9} \text{ GeV cm}^{-2} \text{ s}^{-1} \text{ sr}^{-1}$ , 3.2 (0.6) events are expected at the resonant energy region for 1 year of observation. The off-resonant

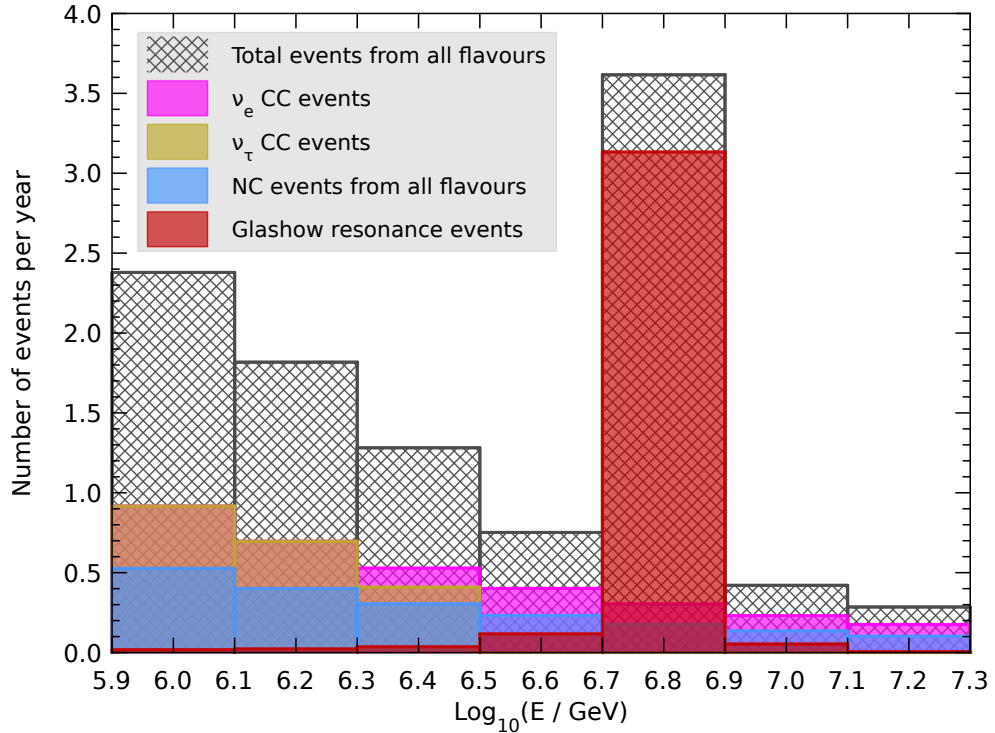


Figure 3.1: The shower spectrum for pure  $pp$  sources,  $x = 1$ . We have neglected events from the interactions  $\bar{\nu}_e e \rightarrow \bar{\nu}_e e$  and  $\bar{\nu}_e e \rightarrow \bar{\nu}_\tau \tau$  which contribute, comparatively, a very tiny fraction of events to the spectrum.

background events receive contributions from  $\nu_e N + \bar{\nu}_e N$  (CC) and  $\nu_\alpha N + \bar{\nu}_\alpha N$  (NC), where CC (NC) represents the charged (neutral) current. The tau contribution  $\nu_\tau N + \bar{\nu}_\tau N$  (CC) is irrelevant at the resonance energy bin since a tau with  $E_\tau \gtrsim 2 \text{ PeV}$  manifests itself as a track. The event rate of  $\nu_e N + \bar{\nu}_e N$  (CC) is given by

$$\text{Rate} = 2\pi N_A V_{\text{eff}} \int dE_\nu [\sigma_{\text{CC}}(\nu N) \Phi_{\nu_e}(E_\nu) + \sigma_{\text{CC}}(\bar{\nu} N) \Phi_{\bar{\nu}_e}(E_\nu)], \quad (3.2)$$

where  $\sigma_{\text{CC}}(\nu N / \bar{\nu} N)$  is the neutrino–nucleon cross section which is  $\approx 1.4 \times 10^{-33} \text{ cm}^2$  at

$E_\nu = 6.3 \text{ PeV}$  [141]. For  $\nu_\alpha N + \bar{\nu}_\alpha N$  (NC), the rate is calculated as

$$\text{Rate} \simeq 2\pi N_A V_{\text{eff}} \sum_{\alpha=e,\mu,\tau} \int_{E_0/\langle y \rangle}^{E_1/\langle y \rangle} dE_\nu [\sigma_{\text{NC}}(\nu N) \Phi_{\nu_\alpha}(E_\nu) + \sigma_{\text{NC}}(\bar{\nu} N) \Phi_{\bar{\nu}_\alpha}(E_\nu)], \quad (3.3)$$

for the shower energy between  $E_0$  and  $E_1$ . Here  $\langle y \rangle$  is the mean inelasticity which is well described by the average value  $\langle y \rangle = 0.26$  at PeV energies. The NC cross section at the resonant peak is  $\approx 6 \times 10^{-34} \text{ cm}^2$ . In the NC process, only a part of the neutrino energy (about 26%) is converted to shower energy, so that the NC contribution is generally small with respect to the CC event number. We have assumed 100% shadowing by the earth for the sake of simplicity, but note that muon and tau neutrinos are not completely attenuated and actually about 20% of them survive in average at the resonant energy. The muon and tau component in Eq. (3.3) would thus receive  $\simeq 20\%$  enhancement in a more precise treatment. For showers with energies  $10^{6.7} \text{ GeV} < E_{\text{shower}} < 10^{6.9} \text{ GeV}$ , for example, the rate reads  $0.31 \text{ yr}^{-1}$  for CC and  $0.18 \text{ yr}^{-1}$  for NC in the case of a  $pp$  flux.

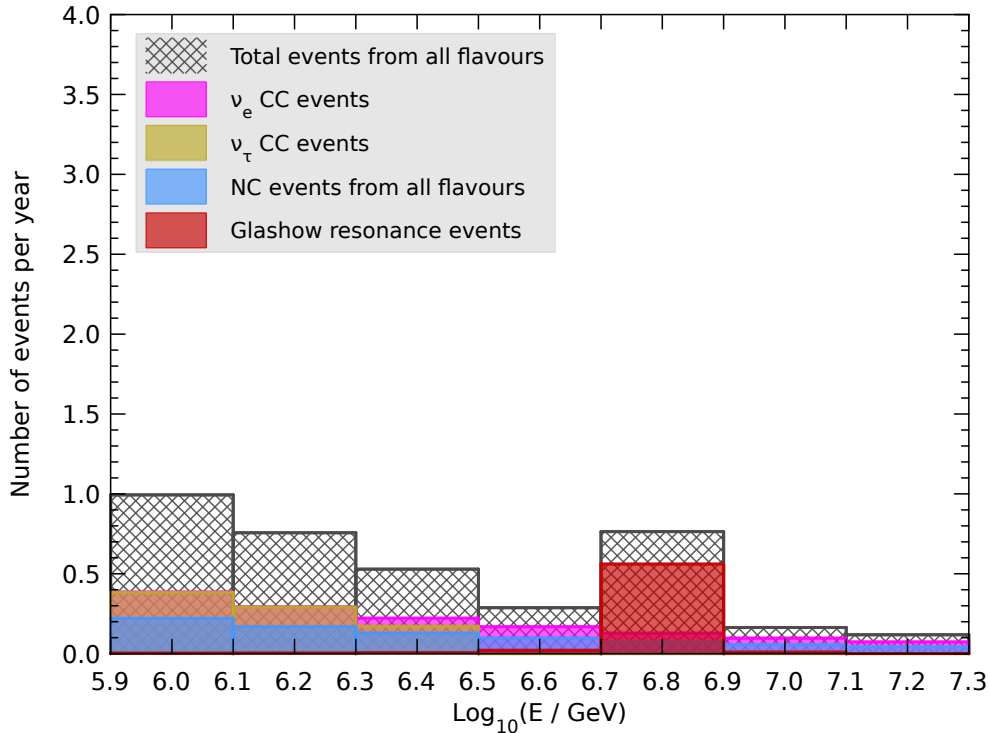


Figure 3.2: The shower spectrum for pure  $p\gamma$  sources,  $x = 0$ . We have neglected events from the interactions  $\bar{\nu}_e e \rightarrow \bar{\nu}_e e$  and  $\bar{\nu}_e e \rightarrow \bar{\nu}_\tau \tau$  which contribute, comparatively, a very tiny fraction of events to the spectrum.

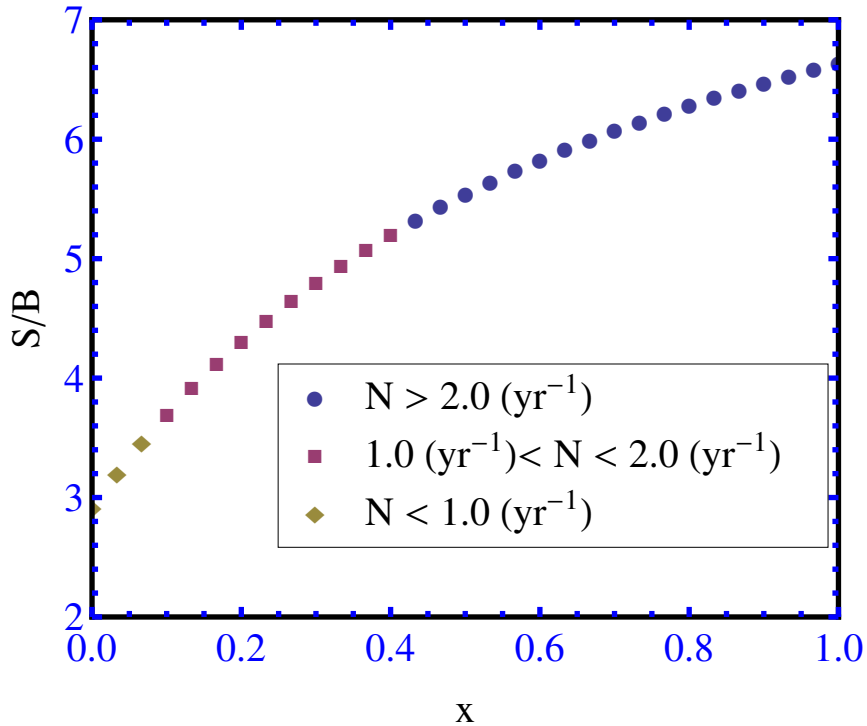


Figure 3.3: The ratio of  $\bar{\nu}_e e \rightarrow \text{hadrons}$  to the off-resonant processes in the resonant bin as a function of  $x$ .  $N$  represents the total number of event in the resonant bin.

Figs. 3.1 and 3.2 show the number of events in the neighborhood of the resonant energy. Fig. 3.1 is for a pure  $pp$  flux with  $x = 1$  and Fig. 3.2 for a pure  $p\gamma$  flux  $x = 0$ . As was pointed out in [135], the resonance peak is clearly seen for a pure  $pp$  source, whereas the peak is significantly weakened for  $p\gamma$  sources. We have divided the energy decade  $10^{6.3} \text{ GeV} < E_{\text{shower}} < 10^{7.3} \text{ GeV}$  into five bins by assuming the energy resolution of the shower to be  $\log_{10}(E_{\text{shower}}/\text{GeV}) = 0.2$ . Notice that  $\nu_\tau N + \bar{\nu}_\tau N$  and  $\nu_e N + \bar{\nu}_e N$  generate the same event numbers at low energies in Fig. 3.1, since the cross section and the  $pp$  fluxes are flavor blind. For energies higher than  $10^{6.5} \text{ GeV}$ , events numbers from  $\nu_\tau N + \bar{\nu}_\tau N$  are lower because the tau track becomes visible and the events can be separated from a single shower. Fig. 3.3 shows the ratio of  $\bar{\nu}_e e \rightarrow \text{hadrons}$  to the sum of all off-resonant processes in the resonant bin  $10^{6.7} \text{ GeV} < E_{\text{shower}} < 10^{6.9} \text{ GeV}$  as a function of  $x$ . The ratio rises from 3 at  $x = 0$  to about 7 at  $x = 1$ .

While the total spectral shape shown in Fig. 3.1 and 3.2 crucially depends on the parameter  $x$ , it also depends on the flavor composition at the earth. For example, if the muon and tau components would evanesce while the (anti-)electron would stay constant, perhaps due to non-standard physical effects affecting the oscillation probabilities, the

ratio of the resonant to off-resonant events is enhanced over the “standard” maximal value set by  $x = 1$ . In an opposite case where only the electron component is damped, the ratio would be anomalously small. Hence the shower spectral shape around the resonance has certain sensitivities to the deformation of the flavor composition, being a complementary test to the shower/muon track ratio.

### 3.2 Novel signatures of the Glashow resonance

We now discuss other unique signatures of the Glashow resonance; the pure muon and the contained lollipop. If the resonant process  $\bar{\nu}_e e \rightarrow \bar{\nu}_\mu \mu$  takes place in the detector volume, it will be observed as a muon track without shower activities at its starting point, see Fig. 2.1. This “pure muon” signature will be clearly distinguishable from the usual muon track from  $\nu_\mu N$  charged current interactions. The probability that the shower associated with the  $\nu_\mu N$  CC process does not reach the detection threshold is extremely small at PeV energies. There is a possibility that bremsstrahlung of the pure muon may distort the signal. However, this bremsstrahlung occurs only about 10% of the time, and the energy fraction carried by the radiation is much smaller than  $\langle y \rangle = 0.26$  of the shower. Therefore the probability that the signal is misidentified as the  $\nu_\mu N \rightarrow \mu X$  is expected to be small. The only remaining candidate for background is thus the muon created by the non-resonant process  $\nu_\mu e \rightarrow \mu \nu_e$ .

The event rate of  $\bar{\nu}_e e \rightarrow \bar{\nu}_\mu \mu$  with the muon energy  $E_0 < E_\mu < E_1$  is calculated by

$$\text{Rate} = 2\pi \frac{10}{18} N_A V \left[ \int_{E_0}^{E_1} dE_\nu \int_{\frac{E_0}{E_\nu}}^1 dy + \int_{E_1}^{\infty} dE_\nu \int_{\frac{E_0}{E_\nu}}^{\frac{E_1}{E_\nu}} dy \right] \frac{d\sigma(\bar{\nu}_e e \rightarrow \bar{\nu}_\mu \mu)}{dy} \Phi_{\bar{\nu}_e}(E_\nu), \quad (3.4)$$

where  $V = 1 \text{ km}^3$  is the instrumental volume of IceCube. The non-resonant process  $\nu_\mu e \rightarrow \mu \nu_e$  is also calculated in the same manner by replacing the cross section and the flux.

Fig. 3.4 shows the event number spectrum of these processes. It is seen that  $\bar{\nu}_e e \rightarrow \bar{\nu}_\mu \mu$  is dominant in the energy regime  $5.0 < \log_{10}(E_\mu/\text{GeV}) < 6.75$ , where the  $\nu_\mu e \rightarrow \mu \nu_e$  contribution is tiny for  $x = 1$ . The integrated number of resonant events in this region is  $0.26 \text{ yr}^{-1}$ . Although the absolute number of the expected event is small, even a single detection of the pure muon event becomes essentially a discovery of the resonance at this energy regime due to its uniqueness. For  $x = 0$ , the rate decreases to  $0.048 \text{ yr}^{-1}$ .

Turning to the contained lollipop, this signature denotes the case when the resonant process  $\bar{\nu}_e e \rightarrow \bar{\nu}_\tau \tau$  takes place in the detector volume and the tau decays a significant distance thereafter, see Fig. 2.2. This will be observed as a tau track popping up inside the detector (without an initial hadronic shower) and a subsequent shower when it decays at the end of the track. It is a “double-bang without the first bang” so to speak. The

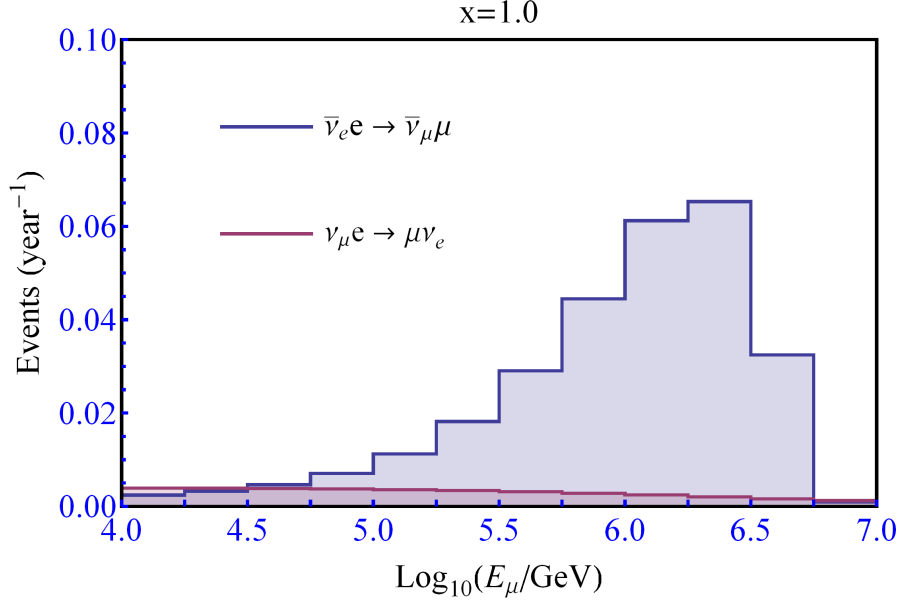


Figure 3.4: The number of pure  $\mu$  events as the functions of the muon energy for a pure  $pp$  source,  $x = 1$ .

event rate with the tau energy of  $E_0 < E_\tau < E_1$  is given by

$$\text{Rate} = 2\pi \frac{10}{18} N_A A \left[ \int_{E_0}^{E_1} dE_\nu \int_{\frac{E_0}{E_\nu}}^1 dy + \int_{E_1}^{\infty} dE_\nu \int_{\frac{E_0}{E_\nu}}^{\frac{E_1}{E_\nu}} dy \right] \frac{d\sigma(\bar{\nu}_e e \rightarrow \bar{\nu}_\tau \tau)}{dy} \Phi_{\bar{\nu}_e}(E_\nu) \times \int_{L_0}^{L_1 - x_{\min}} dx_0 \int_{x_0 + x_{\min}}^{L_1} dx \frac{1}{R_\tau} e^{-\frac{x-x_0}{R_\tau}}, \quad (3.5)$$

where  $R_\tau$  is the tau range  $R_\tau \simeq c\tau y E_\nu / m_\tau$ , and  $A = 1 \text{ km}^2$  is the effective area of the detector,  $L_1 - L_0 = L = 1 \text{ km}$  is the length of the detector,  $x_0$  is the neutrino interaction point, and  $x_{\min}$  is the minimum length to separate the tau decay point from the tau creation point. We take  $x_{\min} = 100 \text{ m}$  as a reference value. The exponential factor accounts for the probability with which a tau created at the point  $x_0$  decays at the point  $x$ .

Fig. 3.5 shows the event spectrum for  $x = 1$  in comparison with the obvious candidate of the background,  $\nu_\tau e \rightarrow \tau \nu_e$ . The contained lollipop dominates in the  $6.0 < \log_{10}(E_\tau/\text{GeV}) < 6.75$  regime. The integrated number of events in this region is  $0.046 \text{ yr}^{-1}$ . As the pure muon case, observation of a single event would essentially become discovery of the resonance. Note however that the expected event number is about five times smaller than the one from the pure muon signature.

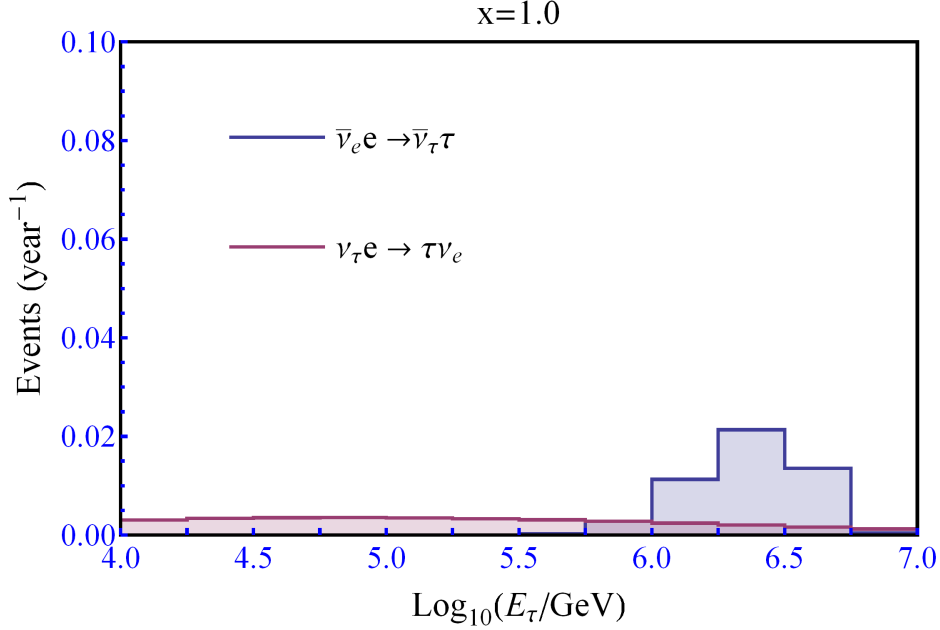


Figure 3.5: The event spectrum of the contained lollipop for a pure  $pp$  source,  $x = 1$ .

Finally let us define the total signal of the Glashow resonance as the sum of shower, muon track and contained lollipop events. That is,

$$N(\text{Shower} + \mu + \tau) \equiv N(\bar{\nu}_e e \rightarrow \text{hadrons}) + N(\bar{\nu}_e e \rightarrow \bar{\nu}_\mu \mu) + N(\bar{\nu}_e e \rightarrow \bar{\nu}_\tau \tau), \quad (3.6)$$

where  $N(\bar{\nu}_e e \rightarrow \text{hadrons})$  is the number of shower events in  $6.7 < \log_{10}(E_{\text{shower}}) < 6.9$  induced by  $\bar{\nu}_e e \rightarrow \text{hadrons}$ ,  $N(\bar{\nu}_e e \rightarrow \bar{\nu}_\mu \mu)$  is the number of pure muon events in  $5.0 < \log_{10}(E_\mu/\text{GeV}) < 6.75$ , and  $N(\bar{\nu}_e e \rightarrow \bar{\nu}_\tau \tau)$  is the number of contained lollipop events in  $6.0 < \log_{10}(E_\tau/\text{GeV}) < 6.75$ . Fig. 3.6 presents the total number of the GR events as a function of  $x$ . The background (*i.e.* the off-resonant contributions) is defined by the summation of the total shower events other than  $\bar{\nu}_e e \rightarrow \text{hadrons}$  in  $6.7 < \log_{10}(E_{\text{shower}}) < 6.9$ , the number of events for  $\nu_\mu e \rightarrow \mu \nu_e$  in  $5.0 < \log_{10}(E_\mu/\text{GeV}) < 6.75$  and for  $\nu_\tau e \rightarrow \tau \nu_e$  in  $6.0 < \log_{10}(E_\tau/\text{GeV}) < 6.75$ . The signal/background ratio rises from  $\simeq 3$  at  $x = 0$  to  $\simeq 7$  at  $x = 1$ . For  $x = 1$ , 7.2 signal events against about 1 background event are expected with 2 years of data accumulation, which is well above the 99% C.L. upper limit for the background only (observation of 1 expected background event corresponds to an upper limit of 5.79 events at 99% C.L. [144]). For  $x = 0.5$ , 6.3 signal events and about 1 background event is expected with 3 years of data accumulation. For the pure  $p\gamma$  case  $x = 0$ , 6.5 signal and about 2 background events are expected within 10 years of data accumulation, which is slightly below the 99% C.L. upper limit for background only

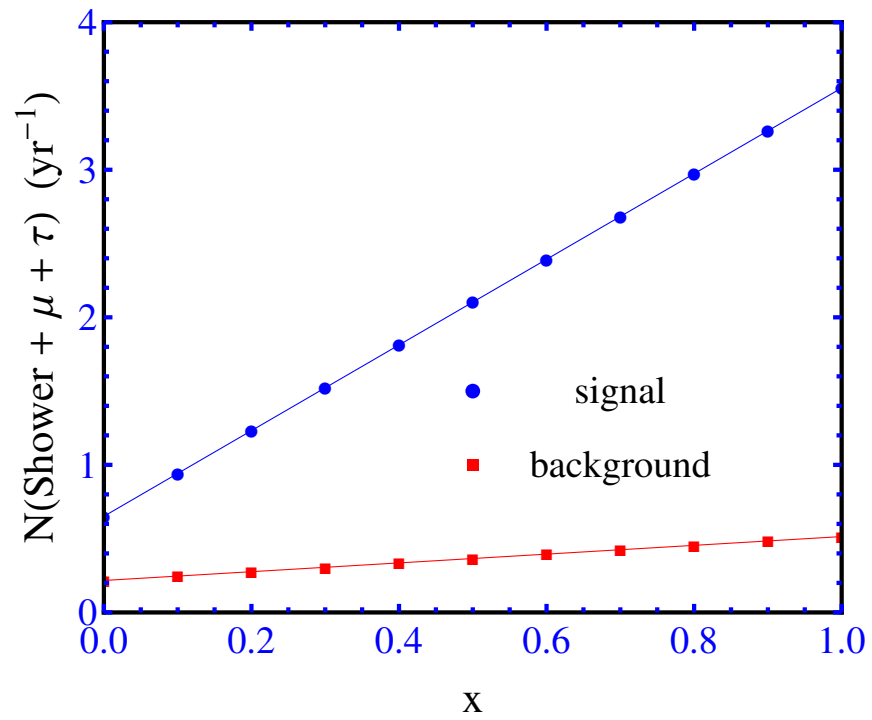


Figure 3.6: Total number of the Glashow resonance signal as a function of  $x$ . The lower (red) curve shows the background (*i.e.* off-resonant processes).

$x$	Non-resonance	GR	Total
0.0	0.21	0.65	0.86
0.5	0.37	2.1	2.5
1.0	0.51	3.6	4.1

Table 3.1: A list of expected numbers of events for 1 year data taking in IceCube.

observation (observation of 2 expected background events corresponds to an upper limit of 6.69 events at 99% C.L. [144]). Table 3.1 shows the non-resonant, Glashow resonance and total number of events for three representative values of  $x$ . Depending on the relative abundance of the  $pp$  and  $p\gamma$  sources, 20, 12 and 4 events are expected in IceCube in 5 years.

Our focus in this section was on signatures and event numbers of the Glashow resonance. From the more general point of view of discovery of high-energy cosmic neutrinos however, the off-resonant events (treated as backgrounds so far) are also signals, being distinctive of neutrinos at energies which could not possibly be produced at any other neutrino source. Atmospheric neutrinos are not a significant background for such a discovery since their fluxes are negligibly low at PeV energies and their contribution, consequently, is insignificant.

### 3.3 Conclusion

We see, therefore, that the Glashow resonance is opportunistically poised with respect to the sensitivity of the IceCube to serve as a probe for the ultra-high energy neutrino flux coming from extra-galactic sources. Besides the standard hadronic/electromagnetic cascade, the pure muon from  $\bar{\nu}_e e \rightarrow \bar{\nu}_\mu \mu$  and the contained lollipop signatures from  $\bar{\nu}_e e \rightarrow \bar{\nu}_\tau \tau$  can be identified as clear signals of the resonance. Applying a Waxman-Bahcall  $E^{-2}$  flux in agreement with recent limits, the event numbers for general  $pp$  and  $p\gamma$  sources indicate that if the neutrino fluxes are positioned with such intensities as presently conjectured, the confirmation of the resonance is possible with several years of data collection at IceCube. The resonance itself could be used as a discovery tool for diffuse astrophysical neutrinos at PeV energies, and to obtain important information about cosmic-rays and astrophysical sources.



## Part III

# Probing Non-Standard Physics with Events at IceCube



# Chapter 4

## Introduction

Neutrinos produced via decay of pions are expected to roughly carry the flavour ratio ( $\nu_e : \nu_\mu : \nu_\tau =$ )  $1 : 2 : 0$  at the source. Standard neutrino oscillations in vacuum massage this ratio during propagation to  $1 : 1 : 1$  [57, 58] at the detector, if we assume  $\theta_{13} = 0$  and  $\theta_{23} = \pi/4$  consistent with current data [59, 60, 61]. As we will show in the following section, standard flavour oscillations over Mega-parsec distances make the neutrino spectra of every flavour nearly identical in shape. Therefore, if for any reason the astrophysics in the source leads to a ratio different from  $1 : 2 : 0$  or spectral shapes for flavours which differ widely from each other, standard oscillations still massage them into identical shapes and magnitudes which are within a factor of roughly 2 of each other by the time they reach the earth.

### 4.1 Spectral Averaging due to Oscillations

Fig. 4.1 (in arbitrary units, and without normalisation) shows the spectra<sup>1</sup> of two flavours in a single source AGN, intentionally chosen to be significantly differing in shape and magnitude, and the resulting diffuse fluxes from all such sources for the same flavours as seen at earth after standard propagation using the procedure described above. It is evident that not only do oscillations tend to bring widely differing magnitudes close (to within a factor of 2) to each other, but they wash out even large differences in spectral shapes that may originate in a particular source, perhaps due to conventional physics, as *e.g.* in [63]. We have checked that this conclusion holds in general, and a common intermediate shape is assumed by both fluxes at earth detectors. These conclusions are no longer true if in the propagation equation, the oscillation probability is modified by new physics in an energy-dependant manner, as we demonstrate in the examples below.

---

<sup>1</sup>The spectra shown here is unrealistic and chosen only to demonstrate the effect of standard oscillations on even such widely differing flavour fluxes.

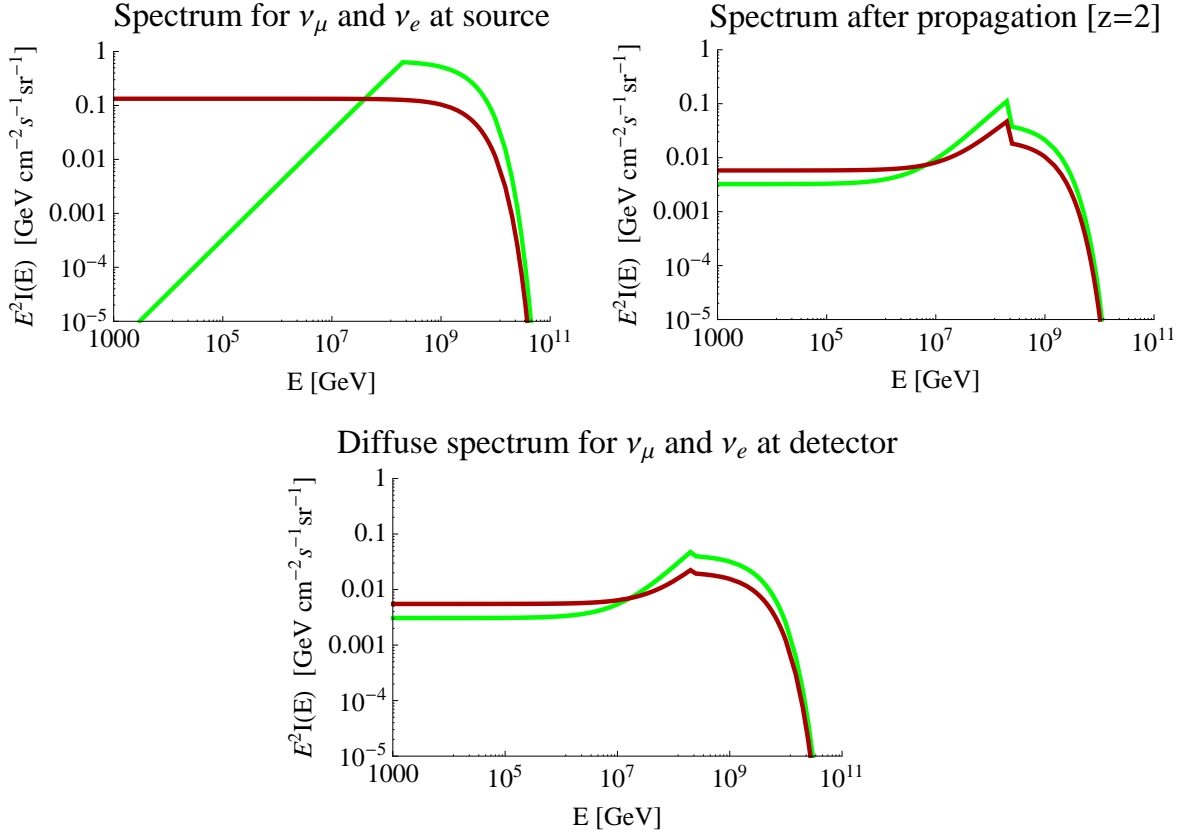


Figure 4.1: The even-ing out of possible spectral distortions present at source due to oscillations over large distances. The green and deep red lines represent assumed spectra from a single (hypothetical) extra-galactic source for the flavours  $\nu_e$  and  $\nu_\mu$  respectively at various stages: (clockwise, starting from the top-left) at the source, at earth from the single source evened out by standard oscillation and finally, the corresponding diffuse fluxes (from similar sources) at earth after integrating over source distribution and oscillations.

# Chapter 5

## Effect of Non-Standard Physics on Neutrino Propagation

A series of papers [64, 65, 66, 67, 68, 69, 70, 71, 72, 73] over the past few years have demonstrated that if the flavour ratios  $\nu_e^d : \nu_\mu^d : \nu_\tau^d$  detected by extant and upcoming neutrino telescopes were to deviate significantly from this democratic prediction, then important conclusions about physics beyond the Standard Model and neutrino oscillation parameters may consequently be inferred. In addition, deviations of these measured ratios have been shown to be sensitive to neutrino oscillation parameters [74, 75, 76, 77, 78, 79, 80, 81, 82, 83, 84, 73] (*e.g.* the mixing angles and the Dirac CP violating phase).

In this chapter we study the spectral distortions in the *diffuse* (*i.e.* integrated over source distribution and redshift) UHE neutrino flux as a probe for the effects of new physics. For specificity, we focus on AGN fluxes, and use, as a convenient benchmark, the well-known upper bounds first derived by Waxman and Bahcall (WB) [85] and later by Mannheim, Protheroe and Rachen (MPR) [86] on such fluxes for both neutron-transparent and neutron-opaque sources (or, equivalently, sources that are *optically thin* and *optically thick*, respectively, to the emission of neutrons). In particular we focus on the upper bounds to the diffuse neutrino flux from hadronic photoproduction in AGN's derived in [86] using the experimental upper limit on cosmic ray protons. All distortions in the fluxes are, as would be expected, transmitted to the upper bounds, thus providing a convenient way of representing and studying them.

As demonstrated in Sec. 4.1, the usual (SM) neutrino oscillations not only tend to equilibrate widely differing source flux magnitudes between flavours, but also massage them into a common spectral shape, as one would intuitively expect. Thus observed relative spectral distortions among flavours are a probe of new physics present in the propagation equation. To demonstrate our approach we then focus on specific cases of non-standard physics, *viz.* *a)* Decay of neutrinos, *b)* The effect of variation of  $\theta_{13}$  and the presence of a non-zero CP-violating phase ( $\delta_{\text{CP}} \neq 0$ ), and *c)* Lorentz violation (LV) in the

neutrino sector. The effect of decoherence among the neutrino flavours during propagation and that of the presence of pseudo-Dirac neutrinos is also briefly discussed. Our method can straightforwardly be applied to other new physics scenarios and our results translated into bounds on muon track versus shower event rates<sup>1</sup> for UHE experiments.

In our calculations throughout this chapter we use the following values of the neutrino mixing parameters [87]:

$$\begin{aligned}\Delta m_{21}^2 &= 7.65 \times 10^{-5} \text{ eV}^2 \\ \Delta m_{31}^2 &= \pm 2.40 \times 10^{-3} \text{ eV}^2 \\ \sin^2(\theta_{12}) &= 0.321, \quad \sin^2(\theta_{23}) = 0.47, \quad \sin^2(\theta_{13}) = 0.003.\end{aligned}$$

The chapter is organized as follows. Section 5.1 shows the modification of these fluxes due to decay of the heavier neutrinos, and its effect on the number of detectable events at a large volume detector like the IceCube. We examine the effect of variation of  $\theta_{13}$  and the CP violating phase  $\delta_{CP}$  in Section 5.2. We look at the effect of Lorentz-symmetry violation in Section 5.3, and finish with brief investigations of the effects of pseudo-Dirac neutrinos and decoherence in the last two sections.

## 5.1 Effect of neutrino decay

### 5.1.1 Introduction to neutrino decay

Bounds on the life-times of neutrinos are obtained primarily from observations of solar [88] and atmospheric neutrinos. Observations from solar neutrinos lead to

$$\frac{\tau_2}{m_2} \geq 10^{-4} \text{ s/eV} \quad (5.1)$$

while, if the neutrino spectrum is normal, the data on atmospheric neutrinos constrain the life-time of the heaviest neutrino

$$\frac{\tau_3}{m_3} \geq 10^{-10} \text{ s/eV}. \quad (5.2)$$

In the following, we treat the lightest neutrino as stable in view of the fact that its decay would be kinematically forbidden, and consider the decay of the heavier neutrinos to invisible daughters like sterile neutrinos, unparticle states, or Majorons. Neutrinos may decay via many possible channels. Of these, radiative two-body decay modes are

---

<sup>1</sup> These count the sum of *a*) neutral current (NC) events of all flavours, *b*) electron neutrino charged current (CC) events at all energies, and *c*)  $\nu_\tau$  induced CC events at energies below  $\leq 1$  PeV ( $10^6$  GeV), whereas muon track events arise from  $\nu_\mu$  induced muons born in CC interactions.

strongly constrained by photon appearance searches [89] to have very long lifetimes, as are three-body decays of the form  $\nu \rightarrow \nu\nu\bar{\nu}$  which are constrained [90] by bounds on anomalous  $Z\nu\bar{\nu}$  couplings [91]. Decay channels of the form

$$\nu_i \rightarrow \nu_j + X \quad (5.3)$$

$$\nu \rightarrow X \quad (5.4)$$

where  $\nu_i$  represents a neutrino mass eigenstate and  $X$  represents a very light or massless invisible particle, e.g. a Majoron, are much more weakly constrained, however and are therefore the basis of our consideration in this section. When considering decays via the channel in Eq. (5.3) we assume that the daughter neutrino produced is significantly reduced in energy and does not contribute to the diffuse flux in the energy range relevant for our purpose (1000 GeV to  $10^{11}$  GeV). A detailed study of the various possible scenarios for neutrino decay is made in [115].

Prior to proceeding, we would like to discuss cosmological observations of high precision which might be able to constrain models of decay via channels as in Eq. (5.3) in the future. These constraints are based on the determination of the neutrino mass scale as discussed in [93], or from the cosmic microwave background as discussed in [111]. Such observations would serve to push the lower bound of neutrino decay lifetimes by several orders of magnitude compared to those discussed here. However, these predictions are dependent upon the number of neutrinos that free-stream and assume couplings of similar nature and strength for all the species of the neutrino family. As discussed in [114] and [94] these assumptions must await confirmation and rely on future data. Hence, “fast” neutrino decay scenarios are not ruled out within the scope of current theory and experiment, though they are disfavoured. Further the decay of neutrinos via Eq. (5.4) and in the cases where the decay, both via Eq. (5.3) and Eq. (5.4) happen due to unparticle scenarios are not covered by such constraints and the purely phenomenological and general study of neutrino decay in the life-times discussed here would still be interesting and relevant for future neutrino detectors.

### 5.1.2 Effect of neutrino decay on the flavour fluxes

A flux of neutrinos of mass  $m_i$ , rest-frame lifetime  $\tau_i$ , energy  $E$  propagating over a distance  $L$  will undergo a depletion due to decay given (in natural units with  $c = 1$ ) by a factor of

$$\exp(-t/\gamma\tau) = \exp\left(-\frac{L}{E} \times \frac{m_i}{\tau_i}\right)$$

where  $t$  is the time in the earth’s (or observer’s) frame and  $\gamma = E/m_i$  is the Lorentz boost factor. This enters the oscillation probability and introduces a dependence on the lifetime and the energy that significantly alters the flavour spectrum. Including the decay factor,

the probability of a neutrino flavour  $\nu_\alpha$  oscillating into another  $\nu_\beta$  becomes

$$P_{\alpha\beta}(E) = \sum_i |U_{\beta i}|^2 |U_{\alpha i}|^2 e^{-L/\tau_i(E)}, \quad \alpha \neq \beta, \quad (5.5)$$

which modifies the flux at detector from a single source to

$$\phi_{\nu_\alpha}(E) = \sum_{i\beta} \phi_{\nu_\beta}^{\text{source}}(E) |U_{\beta i}|^2 |U_{\alpha i}|^2 e^{-L/\tau_i(E)}. \quad (5.6)$$

We use the simplifying assumption  $\tau_2/m_2 = \tau_3/m_3 = \tau/m$  for calculations involving the normal hierarchy (*i.e.*  $m_3^2 - m_1^2 = \Delta m_{31}^2 > 0$ ) and similarly,  $\tau_1/m_1 = \tau_2/m_2 = \tau/m$  for those with inverted hierarchy (*i.e.*  $\Delta m_{31}^2 < 0$ ), but our conclusions hold irrespective of this. The total flux decreases as per Eq. (5.6), which is expected for decays along the lines of Eq. (5.4) and, within the limitations of the assumption made in Sec. 5.1.1, also for Eq. (5.3).

The assumption of complete decay leads to (energy independent) flux changes from the expected  $\nu_e^d : \nu_\mu^d : \nu_\tau^d = 1 : 1 : 1$  to significantly altered values depending on whether the neutrino mass hierarchy is normal or inverted as discussed in [65]. From Fig. 5.1 we note that the range of energies covered by UHE AGN fluxes spans about six to seven orders of magnitude, from about  $10^3$  GeV to  $10^{10}$  GeV. For the “no decay” case, the lowest energy neutrinos in this range should arrive relatively intact, *i.e.*  $L/E \simeq \tau/m \simeq 10^4$  sec/eV. In obtaining the last number we have assumed a generic neutrino mass of 0.05 eV and an average  $L$  of 100 Mpc. On the other hand, if there is complete decay, only the highest energy neutrinos arrive intact, and one obtains *i.e.*  $L/E \simeq \tau/m \leq 10^{-3}$  sec/eV. Thus, a study of the relative spectral features and differences of flavour fluxes at earth allows us to study the unexplored range  $10^{-3} < \tau/m < 10^4$  via decays induced by lifetimes in this range (we have referred to this case as “incomplete decay” in what follows).

To calculate the MPR-like bounds with neutrino decay we use the procedure of Sec. 1.3, but replace the standard neutrino oscillation probability by  $P_{\alpha\beta}$  given in Eq. (5.5) with  $E$  replaced by  $E(1+z)$  to account for red-shifting. Since, unlike standard oscillations,  $P_{\alpha\beta}$  has an energy dependence that does not just average out, the diffuse flux obtained with decay effects differ considerably from the MPR bounds in shape as well as magnitude. Fig. 5.1 shows the effect for both normal and inverted hierarchies with a lifetime of  $\tau_2/m_2 = \tau_3/m_3 = 0.1$  s/eV. We note that the effect of decay in altering the diffuse flux spectrum is especially strong in the case of inverted hierarchy.

Fig. 5.2 shows how the diffuse flux spectral shapes change as the lifetimes of the two heavier mass-eigenstates are varied between  $10^{-3}$  s/eV and 1 s/eV. From the figure it is clear that this ( $10^{-3}$  s/eV – 1 s/eV) is the range of life-times that can be probed by ultra-high-energy detectors looking for spectral distortions in the diffuse fluxes of the three flavours. For lifetimes above 1 s/eV the spectral shapes start to converge and become

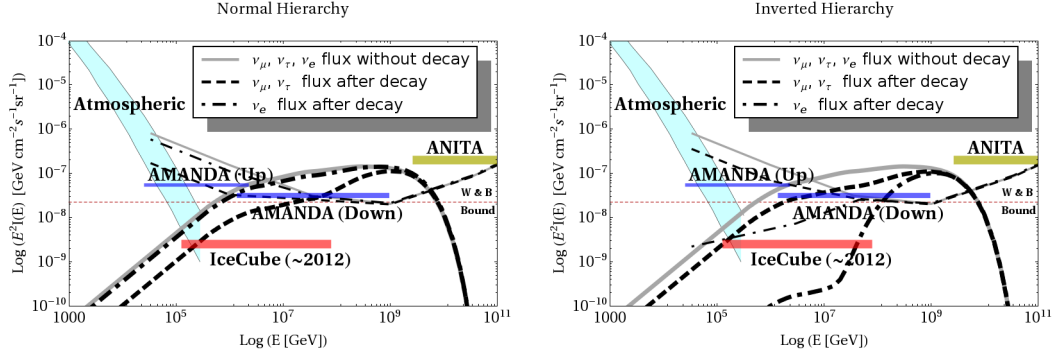


Figure 5.1: Modification of MPR bound for incomplete decay with normal hierarchy (left) and inverted hierarchy (right), and life-time  $\tau_2/m_2 = \tau_3/m_3 = 0.1$  s/eV. The  $\nu_\mu$  and  $\nu_e$  fluxes shown are from optically thick (in thick) and optically thin sources (thinner). Similarly the gray lines indicate the  $\nu_e$ ,  $\nu_\mu$ , or  $\nu_\tau$  undistorted flux modified only by neutrino oscillation, for both optically thick and thin sources. sensitivity thresholds and energy ranges of relevant experiments, *viz.*, AMANDA and IceCube, and ANITA [92] are indicated.  $I(E)$  denotes the diffuse flux spectrum of flavours at earth, obtained as described in the text.

completely indistinguishable beyond  $10^4$  s/eV while for those below  $10^{-3}$  s/eV the shapes of the diffuse fluxes show no difference although their magnitudes are expectedly very different.

As is also the case for complete decays, the results are very different for the two possible hierarchies. This is because the mass eigenstate  $m_1$  contains a large proportion of  $\nu_e$ , whereas the state  $m_3$  is, to a very large extent, just an equal mixture of  $\nu_\mu$  and  $\nu_\tau$  with a tiny admixture of  $\nu_e$ . Therefore decay in the inverted hierarchy case would lead to a disappearance of the eigenstate with high content of  $\nu_e$  and, hence, to its strong depletion against the other two flavours. In the normal hierarchy case, in comparison, the mass eigenstate with the high content of  $\nu_e$  is also the lightest, and decay of the heavier states consequently leads to a depletion of  $\nu_\mu$  and  $\nu_\tau$ . Thus incomplete decay to the lowest mass eigenstate with a normal hierarchy (*i.e.*  $m_1$ ) would lead to considerably more shower events than anticipated with an inverted hierarchy.

While assessing the results presented here, it must be borne in mind that observation of a significant amount of  $\bar{\nu}_e$  from supernova SN1987A possibly imposes lower limits on decay lifetimes of the heavier neutrinos for the inverted hierarchy scenario that are much higher than those considered here [95, 96]. This observation, of a flux of  $\bar{\nu}_e$  roughly in keeping with standard predictions constrains its “lifetime”  $\tau/m > 10^5$ , *i.e.*, higher than what would give observable results with the methods described here. Despite the uncertainties involved with neutrino production from supernovae and the fact that the

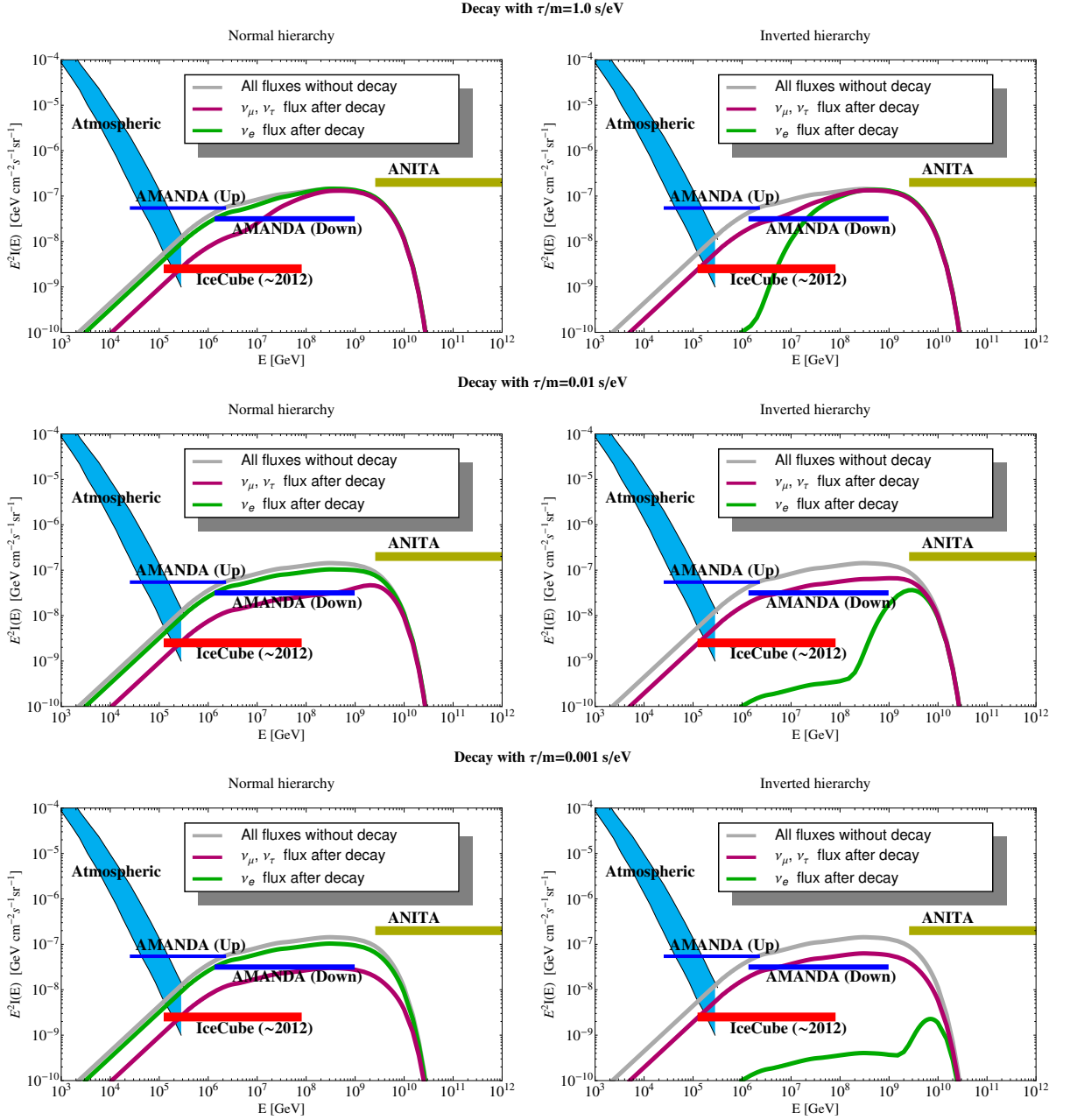


Figure 5.2: Modification of MPR bound for incomplete decay with normal hierarchy (left) and inverted hierarchy (right), and life-times varying from  $\tau/m = 0.001$  s/eV to  $1.0$  s/eV. The  $\nu_\mu$  and  $\nu_e$  fluxes shown are from optically thick sources. The gray lines indicate the  $\nu_e$ ,  $\nu_\mu$ , or  $\nu_\tau$  undistorted flux modified only by neutrino oscillation. Similar effects are seen with fluxes from optically thin sources as well.

total signal from SN1987A was only a handful of events, the results for decay with inverted hierarchy must be judged keeping this in view.

### 5.1.3 Modification of total UHE events due to decay

The effect of decay as seen in the diffuse fluxes in Fig. 5.1 above must also translate to modifications in the shower and muon event rates observable at UHE detectors. In this section we demonstrate this by a sample calculation. We calculate the event-rates induced by the three flavours of high-energy cosmic neutrinos after decay using a simplified version of the procedure in Ref. [116] and compare it to those predicted by standard physics.

Events at the IceCube will be classified primarily into showers and muon-tracks. Shower events are generated due to the charged current (CC) interactions of  $\nu_e$  and  $\nu_\tau$  below the energy of 1.6 PeV and neutral current (NC) interactions of all the three flavours. For energies greater than 1.6 PeV, CC interactions of the  $\nu_\tau$  have their own characteristic signatures in the form of double-bangs, lollipops, earth-skimming events, etc. [97, 98]. Muon-tracks are generated due to the  $\nu_\mu$  induced CC events.

#### $\nu_e$ induced events

In the standard model  $\nu_e$  interacts with nucleons via CC and NC interactions leading to electromagnetic and hadronic showers.

In the CC events, the shower energy is equal to the initial neutrino energy  $E_\nu$ , that is, the total energy of the two final state particles (an electron and a scattered quark). The event rate for  $\nu_e N \rightarrow e^- \chi$ , with  $\chi$  being a final state quark, is given by

$$\text{Rate} = \int_{E_{th}}^{\infty} dE_\nu \int_0^1 dy N_A L \frac{d\sigma_{CC}}{dy} A \mathcal{F}(E_\nu) \quad (5.7)$$

$$= N_A V \int_{E_{th}}^{\infty} dE_\nu \sigma_{CC}(E_\nu) \mathcal{F}(E_\nu) \quad (5.8)$$

where

- $E_\nu$ : the incident neutrino energy
- $E_{th}$ : detection threshold for shower events
- $y$ : the inelasticity parameter defined as  $y \equiv 1 - \frac{E_{e,\mu,\tau}}{E_\nu}$
- $A, L, V$ : the area, length and volume of the detector respectively
- $\mathcal{F}(E_\nu)$ : the flux spectrum of neutrinos in  $\text{GeV}^{-1} \text{cm}^{-2} \text{s}^{-1}$

It is assumed that the electron range is short enough such that the effective volume of the detector is identical to the instrumental volume. Using standard tabulated values of the cross-section  $\sigma_{CC}$  [99, 100] it is straightforward to evaluate the integral in Eq. (5.8) to obtain the event rate. The event rate for anti-neutrino process  $\bar{\nu}_e N \rightarrow e^+ \chi$  is calculated similarly.

For the NC events, the final state neutrino develops into missing energy, so that the rate is given by

$$\text{Rate} = \int_{E_{th}}^{\infty} dE_\nu \int_{\frac{E_{th}}{E_\nu}}^1 dy N_A L \frac{d\sigma_{NC}}{dy} A\mathcal{F}(E_\nu) \quad (5.9)$$

To simplify Eq. (5.9) we use the approximation

$$\frac{d\sigma}{dy} \approx \sigma \delta(y - \langle y \rangle) \quad (5.10)$$

where  $\langle y \rangle$  is the mean inelasticity parameter. Thus, we have

$$\text{Rate} = N_A V \int_{E'_{th}}^{\infty} dE_\nu \sigma_{NC}(E_\nu) \mathcal{F}(E_\nu), \quad (5.11)$$

$E'_{th}$  is an effective threshold energy at which the curves defined by  $y = E_{th}/E_\nu$  and  $y = \langle y \rangle$  intersect.

### $\nu_\mu$ induced events

The muon track event is calculated by

$$\int_{E_{th}}^{\infty} dE_\nu N_A \int_0^{1-\frac{E_{th}}{E_\nu}} dy R(E_\nu(1-y), E_{th}) \frac{d\sigma_{CC}}{dy} S(E_\nu) A\mathcal{F}(E_\nu), \quad (5.12)$$

where,

$$R(x, y) = \frac{1}{b} \ln \left( \frac{a + bx}{a + by} \right) \quad (5.13)$$

with  $a = 2.0 \times 10^{-3} \text{ GeV cm}^{-1}$  and  $b = 3.9 \times 10^{-6} \text{ GeV cm}^{-1}$ .  $S(E_\nu)$  represents the shadowing effect by the earth [99, 100].

Approximating using Eq. (5.10) gives

$$\text{Rate} = \int_{E'_{th}}^{\infty} dE_\nu N_A R(E_\nu(1 - \langle y \rangle), E_{th}) \sigma_{CC}(E_\nu) S(E_\nu) A\mathcal{F}(E_\nu) \quad (5.14)$$

with  $E'_{th}$  being determined similarly as for the  $\nu_e$  induced events.

Using the procedure described above, we calculate the total shower and muon-track detector events (for  $\bar{\nu} + \nu$ ) for the inverted hierarchy scenario with a life-time of 1.0 s/eV depicted in Fig. 5.2 (top-right) and compare it to the events expected from standard physics. The results are tabulated in Table 5.1 where we show event rates for UHE detectors, like the IceCube, over a 10 year period integrated over solid angle. The difference between the ratio of muon-track to shower events due to standard oscillation and that after considering neutrino decay are shown in Fig. 5.3.

Energy [GeV]	Shower		Muon Track	
	No Decay	Decay	No Decay	Decay
$10^3 - 10^4$	7	2	10	5
$10^4 - 10^5$	42	11	96	42
$10^5 - 10^6$	145	36	325	143
$10^6 - 10^7$	129	24	297	134
$10^7 - 10^8$	64	31	85	53
$10^8 - 10^9$	21	19	16	14
$10^9 - 10^{10}$	3	3	1	1
$10^{10} - 10^{11}$	0	0	0	0

Table 5.1: Total shower and muon-track detector events (for  $\bar{\nu} + \nu$ ) over 10 years, and integrated over solid angle for the inverted hierarchy scenario with a life-time of  $\tau/m = 1.0$  s/eV depicted in Fig. 3.

The disappearance of a majority of shower events (due to the depletion of the  $\nu_e$  flux compared to that of  $\nu_\mu$ ) at lower energies, and their reappearance at higher energies is a distinctive feature. It indicates the presence of new physics (like incomplete decay) as opposed to spectral distortions originating in the source, or the appearance of a new class of sources. In the latter case, a corresponding depletion and subsequent enhancement is expected in muon events. By contrast, in the case of incomplete decay the fluxes return to the democratic ratio at higher energies where the neutrinos do not decay.

## 5.2 Effect of non-zero CP violating phase and $\theta_{13}$ variation on neutrino decay

As described in Sec. 5.1 the calculation for the effect of decay of heavier neutrinos on the diffuse flux spectrum was done keeping the CP violating phase  $\delta_{CP} = 0$  and  $\theta_{13}$  at the  $3\sigma$  best fit value which is close to zero. In this section we look at how our conclusions are affected if we change these parameters significantly. In Sec. 5.2.1 we look at how

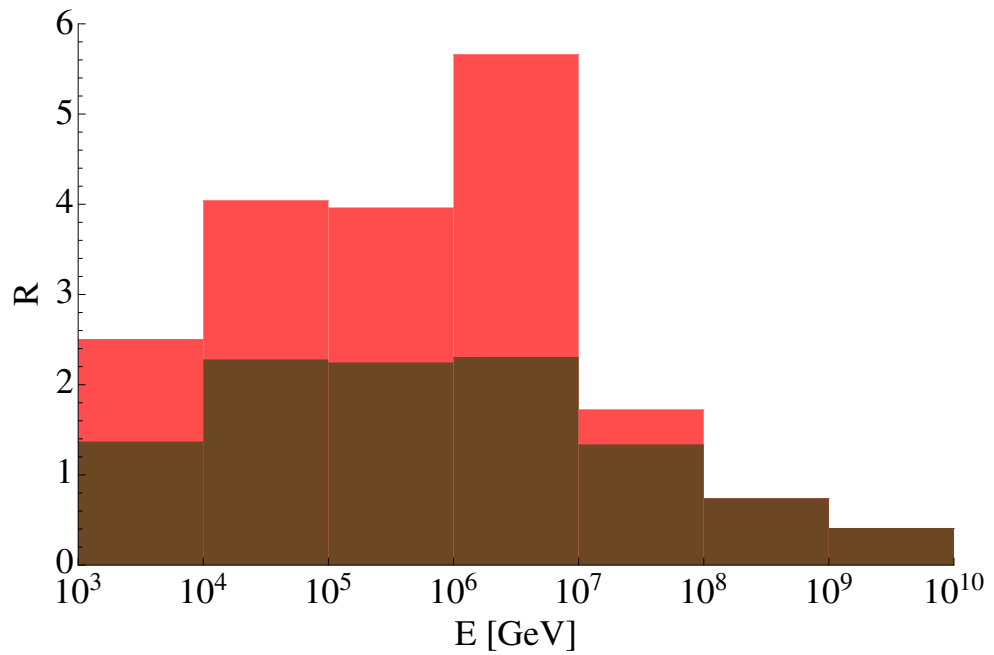


Figure 5.3: The ratio ( $R$ ) of muon-track events to shower events with inverted hierarchy and life-time  $\tau/m = 1.0$  s/eV as shown in Table 1. The ratio expected due to standard physics is shown in brown, while the modified ratio due to the effects of decay is shown in light red. At energies greater than  $10^8$  GeV,  $R$  due to standard physics and that after considering decay become equal.

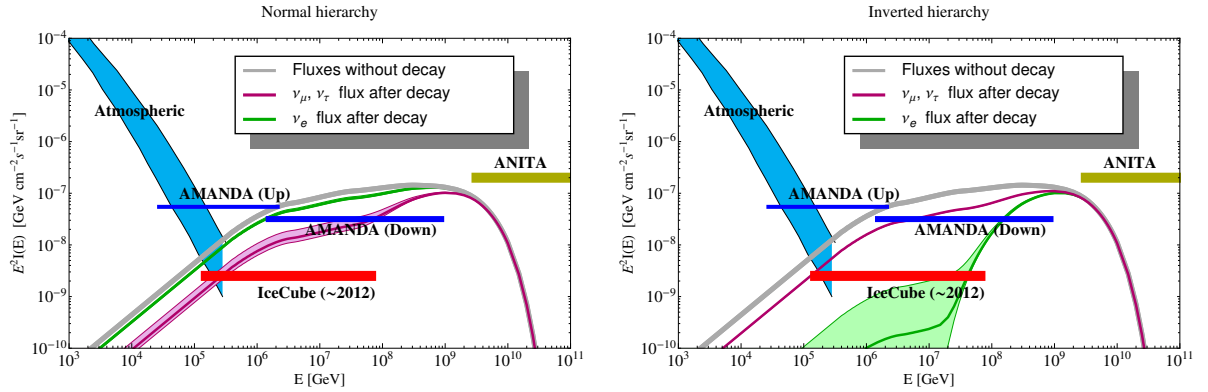


Figure 5.4: Effect of variation of  $\theta_{13}$  over the complete range on decay plots obtained in Fig. 2 using optically thick sources. The shaded regions indicate the area spanned by the diffuse flux spectra as  $\theta_{13}$  varies from 0 to the CHOOZ maximum, while the thick lines represent the spectra obtained with the  $3\sigma$  best-fit value of  $\theta_{13}$ .

changing  $\theta_{13}$  from 0 to the CHOOZ maximum affects the decay effected diffuse fluxes, while in Sec. 5.2.2 we examine the consequences of a non-zero CP violating phase in the same context.

### 5.2.1 Variation of $\theta_{13}$

Observations at CHOOZ [101] constrain the maximum value of  $\theta_{13}$  (90 % confidence level) such that

$$\sin^2(2\theta_{13}^{\max}) = 0.10.$$

Therefore, we have for  $\theta_{13}$  the following experimentally allowed range of values

$$0 \leq \theta_{13} \leq 9.1^\circ$$

We allow  $\theta_{13}$  to vary within this range and study its effect on the results of Sec. 5.1. The results are represented in Fig. 5.4. It is clear that the effect of varying  $\theta_{13}$  is significant. However, given the strong difference in the diffuse flux spectra for inverted and normal hierarchies, variation of  $\theta_{13}$  over the entire range would not affect our qualitative conclusions in Sec. 5.1 regarding differentiating between the two.

### 5.2.2 Non-zero CP violating phase.

The CP violation phase in the three family neutrino mixing matrix is as yet not experimentally determined. Neutrino telescopes probing ultra-high energies might be able to

improve upon our present knowledge of this parameter (see [82], for example). Here we look at how the presence of a non-zero CP violating phase,  $\delta_{CP}$  in the mixing matrix could affect results obtained in Sec. 5.1.

$\delta_{CP}$  enters the oscillation probability via the mixing matrix as the product  $\sin(\theta_{13}) \cdot \exp(\pm i\delta_{CP})$ . Therefore, a non-zero CP violating phase does not affect any of our calculations if  $\theta_{13} = 0$  and its effect is imperceptible even when the  $3\sigma$  best-fit value of  $\theta_{13}$  is used as is the case in Sec. 5.1. For the remainder of this section we keep  $\theta_{13}$  at the CHOOZ maximum and vary the CPV phase from 0 to  $\pi$ . Fig. 5.5 shows the result on the  $\nu_\mu$  flavour for decay in the case of a normal hierarchy for diffuse flux from optically thick sources. In the same way Fig. 5.6 shows the effect of a non-zero CP violating phase on decay with both the normal and inverted hierarchy. The effect of CP violation is quite small on the diffuse flux with inverted hierarchy as compared to that with normal hierarchy.

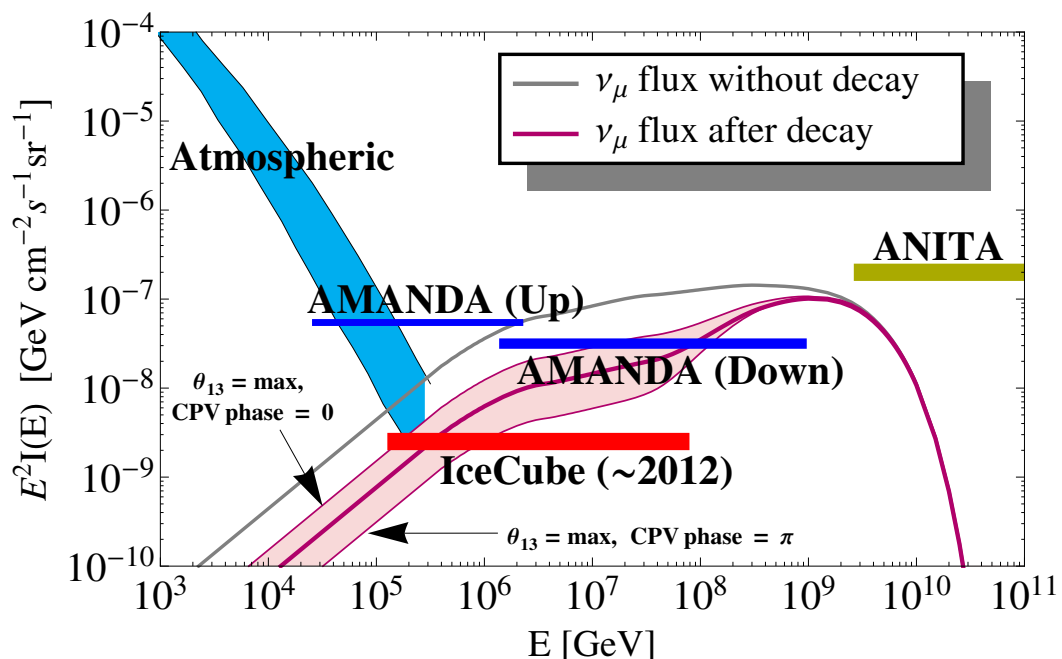


Figure 5.5: Effect of CP violation on the diffuse flux of the  $\nu_\mu$  flavour obtained by considering decay with normal hierarchy and life-time of  $\tau/m = 0.1$  s/eV. The variation in the flux as the CP violating phase is varied between  $0 - \pi$  is shown as the shaded region.

To summarise, it is clear from the discussion in Sec. 5.1 and 5.2 that future neutrino detectors capable of distinguishing between flavours should be able to probe and potentially provide stronger bounds on decay lifetimes of heavier neutrinos. If the neutrinos decay with a lifetime within the ranges discussed here, then they would also be able to distinguish between the two hierarchies due to the strongly different diffuse flux spectra

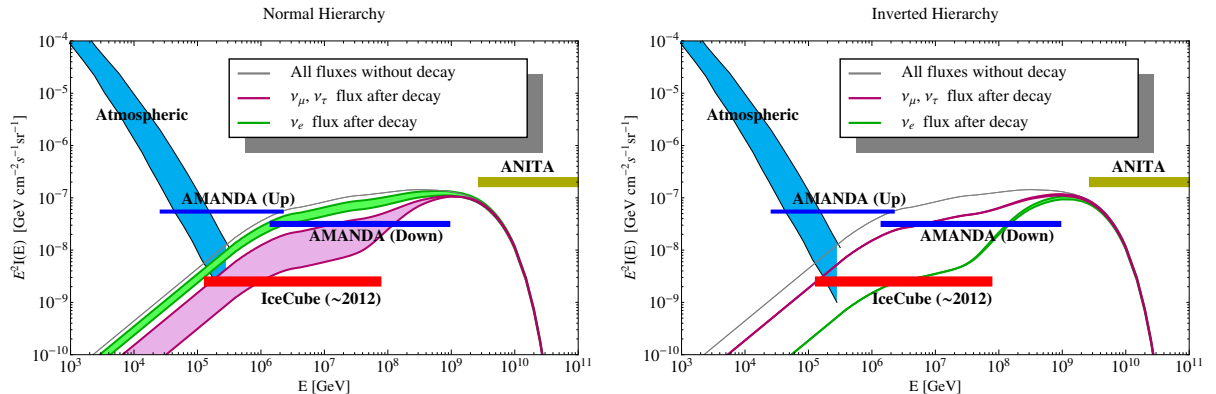


Figure 5.6: Effect of CP violation on fluxes affected by decay for both normal and inverted hierarchies. The shaded regions represent the span of the flux bounds when the CP violating phase is varied from 0 to  $\pi$ , keeping the  $\theta_{13}$  at the CHOOZ maximum.

the two hierarchies lead to for the flavours  $\nu_e$  and  $\nu_\mu$ , notwithstanding the effect of a non-zero CP violating phase or the uncertainty over the value of  $\theta_{13}$ .

### 5.3 Effect of Lorentz symmetry violation

Low energy phenomenology can be affected by Lorentz symmetry violating effects originating at very high energies. Typically such effects originate at energies close to the Planck scale. They may appear in certain theories which are low energy limits of string theory [102, 103], or could possibly signal the breakdown of the CPT theorem [104]. Additionally, if quantum gravity demands a fundamental length scale, leading to a breakdown of special relativity, or loop quantum gravity [105, 106, 107, 112, 108, 109] leads to discrete space-time, one expects tiny LV effects to percolate to lower energies. UHE neutrinos, with their high energies and long oscillation baselines present a unique opportunity for testing these theories. Their effects in the context of flavour flux ratios have been discussed in [70]. They may arise, for example, due to a vector or tensor field forming a condensate and getting a vacuum expectation value, thereafter behaving like a background field. The effective contribution of such background fields can then be handled in the low energy theory using standard model extensions [103]. It has been shown [104] that although CPT symmetry violation implies Lorentz violation, Lorentz violation does not necessarily require or imply the violation of CPT symmetry. In this section we focus on the modification of the propagation of neutrinos due to Lorentz symmetry violating effects along the lines discussed in Ref. [110]. Since the effects of Lorentz-violation and CPT violation are understandably tiny at low energies, it is difficult to explore their phenomenological signatures using low energy probes, in colliders for example. Since they

originate in extremely energetic cosmological accelerators and propagate over cosmic distances, ultra-high energy neutrinos provide the perfect laboratory for constraining and, possibly, determining Lorentz-violating parameters.

### 5.3.1 Modification of neutrino transition probabilities due to LV effects

As an example, we will study, for the simplification that it provides, a two-flavour scenario with massive neutrinos and consider the modification of the transition probability from one flavour to the other by Lorentz-violation due to an effective standard model extension. Our focus is on LV from off-diagonal terms in the effective hamiltonian describing the propagation of the neutrinos [70].

We consider an effective Hamiltonian describing neutrino propagation

$$H_{\alpha\beta}^{\text{eff}} = |\vec{p}| \delta_{\alpha\beta} + \frac{1}{2|\vec{p}|} [\tilde{m}^2 + 2(a^\mu p_\mu)]_{\alpha\beta} \quad (5.15)$$

where  $\tilde{m}$  is related to the neutrino mass and  $a$  is a real CPT and Lorentz violating parameter. In the two neutrino mass basis this gives

$$H_{\text{eff}} = \begin{pmatrix} \frac{m_1^2}{2E} & a \\ a & \frac{m_1^2}{2E} \end{pmatrix}. \quad (5.16)$$

With the mixing angle between the two flavours  $\theta_{23} = \pi/4$ , this modifies the probability of transition from one flavour to another during propagation to

$$P[\nu_\mu \rightarrow \nu_\tau] = \frac{1}{4} \left( 1 - \frac{a^2}{\Omega^2} - \frac{\omega^2}{\Omega^2} \cos(2\Omega L) \right) \quad (5.17)$$

where  $\omega = \frac{\Delta m^2}{4E}$  and  $\Omega = \sqrt{\omega^2 + a^2}$ .

### 5.3.2 Effect of Lorentz violation on neutrino flavour fluxes

To calculate the diffuse fluxes of the two neutrino flavours we use Eq. (5.17) instead of the standard oscillation probability and integrate over the red-shift  $z$ . The probability above contributes a  $z$  dependent term through its dependence on energy. Further the  $\cos(2\Omega L)$  term averages out and consequently does not contribute.

The results of including Lorentz violation in the propagation phenomenology of neutrinos are shown in Fig. 5.7. It is clear from these plots that the strong departure of diffuse spectral shapes of  $\nu_\mu$  and  $\nu_\tau$  from the symmetry expected under standard oscillation

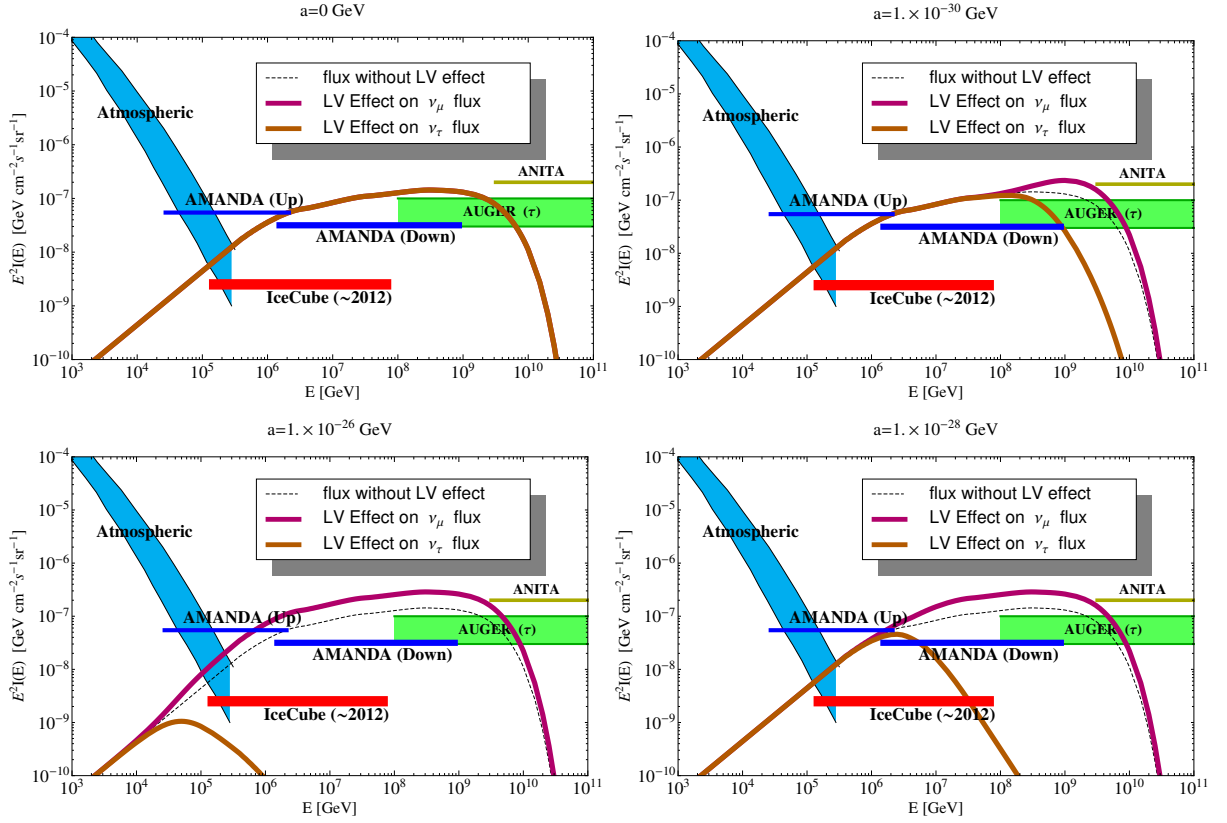


Figure 5.7: Effect of Lorentz violation on the  $\nu_\mu - \nu_\tau$  diffuse flux with various values of the lorentz violating parameter  $a$  (in GeV). Clockwise from top-left (i)  $a = 0$ , (ii)  $a = 10^{-30}$ , (iii)  $a = 10^{-28}$ , (iv)  $a = 10^{-26}$ . The plots show how an increase in the LV parameter results in depletion of the  $\nu_\tau$  flux at progressively lower energies. For the Auger experiment, sensitivities for  $\nu_\tau$  detection using the most pessimistic systematics (top line) and the most optimistic systematics (bottom line) are indicated [113].

phenomenology with  $\theta_{23} = 45^\circ$  is a unique signature of Lorentz-violation. This would lead to a significant decrease in the signature  $\nu_\tau$  events at high energies, like “double-bang”, “lollipop” and “earth-skimming” events as compared to muon-track events. Differences in shape between the two flavours can be seen for  $a < 10^{-30}$  GeV. We have used the case where  $a$  is independent of energy, however if the parameter  $a \propto E^n$  the results would be qualitatively similar to that obtained here but involve significantly different ranges of values for the parameter as expected.

### 5.3.3 Detectability of Lorentz-violation

Unlike in neutrino decay, the effect of Lorentz violation is seen in the deviation of the flux spectra of both the  $\nu_\mu$  and, more strikingly, the  $\nu_\tau$  flavour, from the standard fluxes toward the higher end of the spectrum. This makes it especially interesting for probe by detectors, such as ANITA and the Pierre Auger Observatory [113, 117] having sensitivity to  $\nu_\tau$  in the energy range  $10^8 - 10^{11}$  GeV. While Auger can separate out the  $\nu_\tau$  events, ANITA detects the sum of all three flavours. As is clear from the experimental thresholds shown in Fig. 5.7, should even tiny Lorentz-violation effects exist, both these experiments will, in principle, be able to detect it via lack of characteristic  $\tau$  events expected at these energies from standard physics. As they collect more data in the future, expectedly bringing the corresponding thresholds down, the ability of such experiments to detect tiny LV effects will be gradually enhanced.

## 5.4 Pseudo-Dirac neutrinos

Masses for neutrinos can be generated by extending the Standard model to include right-handed sterile neutrinos to the particle spectrum. The generic mass term for neutrinos becomes

$$\mathfrak{L} = -\frac{1}{2}\overline{\Psi^C}M\Psi + h.c., \quad (5.18)$$

where considering 3 right-handed neutrinos in the spectrum

$$\Psi = \left( \nu_{eL}, \nu_{\mu L}, \nu_{\tau L}, (\nu_{1R})^C, (\nu_{2R})^C, (\nu_{3R})^C \right),$$

and  $\nu^C = \mathcal{C}\overline{\nu}^T$ ,  $\mathcal{C}$  being the charge conjugation operator.

The mass matrix  $M$  is of the form

$$M = \begin{pmatrix} m_L & m_D^T \\ m_D & m_R^* \end{pmatrix}, \quad (5.19)$$

and for  $m_L = m_R = 0$  reduces to neutrino states with Dirac mass. In this case the six

neutrinos decompose into three active-sterile pairs of neutrinos degenerate in mass with maximal mixing angle  $\theta = \pi/4$  for each pair. Due to the mass degeneracy within the neutrinos in such a pair, an active neutrino cannot oscillate into a sterile neutrino from the same pair.

Instead, neutrinos may be pseudo-Dirac states [68] where  $m_L$  and  $m_R$  are tiny but non-zero, i.e.  $m_L, m_R \ll m_D$ . This lifts the degeneracy in mass within an active-sterile pair, and gives a mixing angle  $\theta \approx \pi/4$  between its members. The result of the lifting of this degeneracy is to enable oscillation among species that was not possible in the pure Dirac neutrino case.

The presence of non-zero  $m_L, m_R$  changes the probability of transition of one active state to another during propagation. The expression for the probability for neutrinos propagating over cosmological distances (after various phase factors involving terms like  $\Delta m_{\odot}^2/L$  average out) is [68]

$$P_{\alpha\beta} = \sum_{j=1}^3 |U_{\alpha j}|^2 |U_{\beta j}|^2 \cos^2 \left( \frac{\Delta m_j^2 L}{4E_\nu} \right), \quad (5.20)$$

where  $\Delta m_j^2 = (m_j^+)^2 - (m_j^-)^2$  is the mass squared difference between the active and sterile states in the  $j^{\text{th}}$  pair.

There has been a recent study [118] that explores the pseudo-Dirac scenario at neutrino telescopes using the ratio of shower to muon-track events. Here, we look at distortion of spectral shape from the standard diffuse flux due to the modification of the oscillation probability to Eq. (5.20). We use Eq. (5.20) instead of the standard oscillation probability, otherwise following the same procedure used to derive the standard MPR flux (the base flux in our plots). The results are shown in Fig. 5.8 which shows a decrease in the affected flux at lower energies and rise at the higher end of the spectrum to merge with the standard flux. However, the decrease is only to about half the base flux, and the rise at higher energies is not steep. Therefore, it would be very difficult to detect such an effect in future detector experiments.

## 5.5 Effect of decoherence during neutrino propagation

Quantum decoherence arises at the Planck scale in theories where CPT invariance is broken independently of Lorentz symmetry due to loss of unitarity and serves to modify the time evolution of the density matrix [70, 69]. Though not expected in a majority of string theories, a certain class of string theories called noncritical string theories may allow for decoherence.

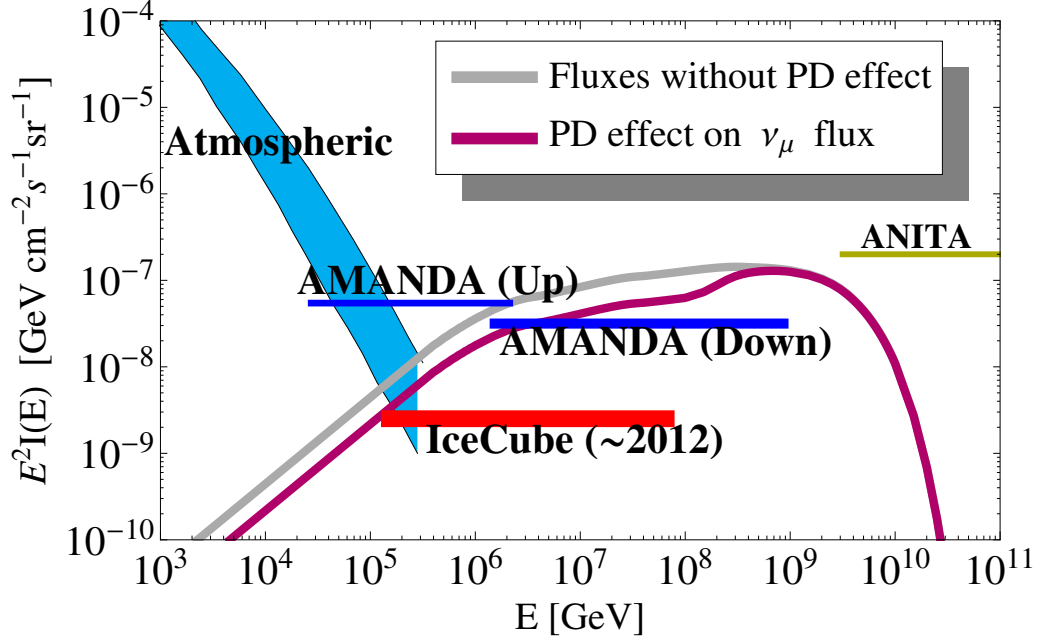


Figure 5.8: Effect of pseudo-Dirac (PD) neutrinos on the  $\nu_\mu$  diffuse flux with  $\Delta m^2 = 10^{-14} \text{ eV}^2$ .

In the context of neutrino oscillation, decoherence serves to modify the transition probabilities among the three flavours. While a general treatment discussing how this happens for the three family case is complicated, we work under the simplifying conditions assumed in [70, see Sec IV.B] to arrive at the transition probability

$$P[\nu_p \rightarrow \nu_q] = \frac{1}{3} + \frac{1}{6} e^{-2\delta L} \left[ 3 (U_{p1}^2 - U_{p2}^2) (U_{q1}^2 - U_{q2}^2) + (U_{p1}^2 + U_{p2}^2 - 2U_{p3}^2) (U_{q1}^2 + U_{q2}^2 - 2U_{q3}^2) \right], \quad (5.21)$$

where  $\delta$  is the only decoherence parameter. This leads to a flavour composition at the detector given by

$$R_{\nu_e} = P[\nu_e \rightarrow \nu_e] \frac{\Phi_{\nu_e}}{\Phi_{\text{TOT}}} + P[\nu_\mu \rightarrow \nu_e] \frac{\Phi_{\nu_\mu}}{\Phi_{\text{TOT}}} + P[\nu_\tau \rightarrow \nu_e] \frac{\Phi_{\nu_\tau}}{\Phi_{\text{TOT}}}, \quad (5.22a)$$

$$R_{\nu_\mu} = P[\nu_e \rightarrow \nu_\mu] \frac{\Phi_{\nu_e}}{\Phi_{\text{TOT}}} + P[\nu_\mu \rightarrow \nu_\mu] \frac{\Phi_{\nu_\mu}}{\Phi_{\text{TOT}}} + P[\nu_\tau \rightarrow \nu_\mu] \frac{\Phi_{\nu_\tau}}{\Phi_{\text{TOT}}}, \quad (5.22b)$$

$$R_{\nu_\tau} = P[\nu_e \rightarrow \nu_\tau] \frac{\Phi_{\nu_e}}{\Phi_{\text{TOT}}} + P[\nu_\mu \rightarrow \nu_\tau] \frac{\Phi_{\nu_\mu}}{\Phi_{\text{TOT}}} + P[\nu_\tau \rightarrow \nu_\tau] \frac{\Phi_{\nu_\tau}}{\Phi_{\text{TOT}}}, \quad (5.22c)$$

where  $\Phi_e/\Phi_{\text{TOT}}$ , etc. are flux composition ratios at source.

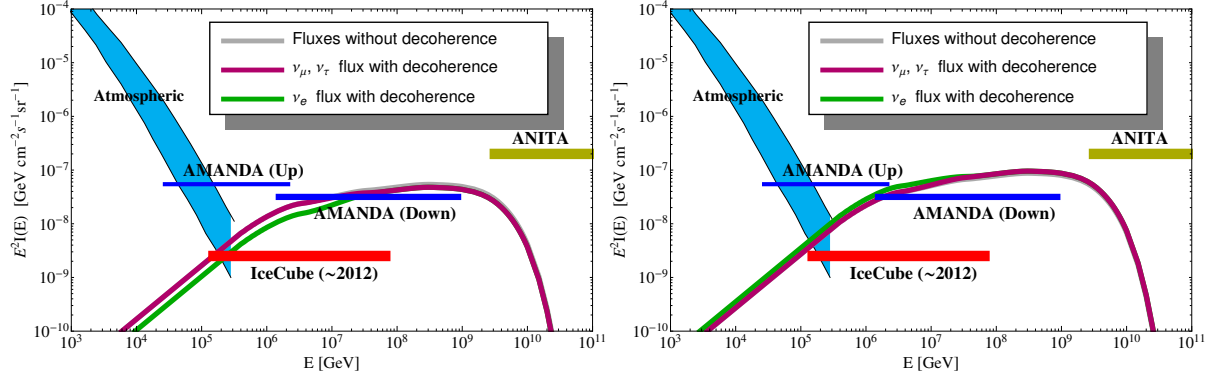


Figure 5.9: Effect of decoherence on the diffuse flux with the parameter  $\delta = \alpha E^2$  and  $\alpha = 10^{-40} \text{ GeV}^{-1}$ . A base flux composition of  $0 : 1 : 0$  corresponding to  $\bar{\nu}$  (*left*) and  $1 : 1 : 0$  corresponding to  $\nu$  (*right*) from pion decay is used for the calculation. It is clear from the figure that (anti-)neutrinos from pion decay are not useful probes for decoherence.

We use the flavour ratios given by Eq. (5.22) to calculate the diffuse flux spectra of each flavour arriving at the detector. The effect of decoherence is to bring the flavour fluxes close to the ratio  $1 : 1 : 1$ . If we use the standard flux from AGN's ( $1 : 2 : 0$  at source) then standard neutrino oscillation already brings the ratio to the above value as discussed in Sec. 4.1 and this makes it difficult to distinguish between the effects of decoherence and standard oscillation. However, if we have detection capabilities that can distinguish between neutrinos and anti-neutrinos, it might be worth investigating decoherence using the differences in flavour spectral shapes. As discussed earlier pion decays in the source via  $\pi^+ \rightarrow \nu_\mu \mu^+$  and subsequently,  $\mu^+ \rightarrow e^+ \bar{\nu}_\mu \nu_e$  contribute to a flavour spectral ratio of  $1 : 1 : 0$  for  $\nu$  and  $0 : 1 : 0$  for  $\bar{\nu}$ . Due to standard oscillation these flavour ratios are reduced to  $0.78 : 0.61 : 0.61$  and  $0.22 : 0.39 : 0.39$  at the detector respectively. Since the effect of decoherence is to reduce the flavour ratios to  $1 : 1 : 1$  irrespective of ratios at source, the transition from the flux due to dominance of standard oscillation to that due to dominance of decoherence might happen within the energy range relevant for our purposes, for a certain range of values of the decoherence parameter. However the effect is almost invisible even if  $\nu$  and  $\bar{\nu}$  fluxes are used as probes, the reason being that the fluxes ratios at detector due to standard oscillation for both (*i.e.*,  $0.78 : 0.61 : 0.61$  and  $0.22 : 0.39 : 0.39$  respectively) are already quite close to the  $1 : 1 : 1$  that decoherence would result in. Effective probe for decoherence are high energy neutrinos from neutron decay, for instance, which gives a flux ratio of  $1 : 0 : 0$  at source [116], and not neutrinos from pion decay. The results for  $\bar{\nu}$  and  $\nu$  with a particular choice of the decoherence parameter is shown in Fig. 5.9. For our calculation, we have chosen the parameter  $\delta \propto E^2$

which is expected within the context of string theories<sup>2</sup>. Upper limits on such a parameter are got from the Super-Kamiokande as  $\sim 10^{-10}$  GeV.

---

<sup>2</sup>The choice of  $\delta \propto E^2$  also violates Lorentz symmetry which introduces weaker secondary effects not taken into account here.

**Part IV**  
**Conclusion**



The detection of UHE neutrinos is imminent. Several detectors will progressively sharpen their capabilities to detect neutrino flavours, beginning with ICECUBE's ability to separate muon tracks from shower events. We have shown that spectral changes in diffuse UHE neutrino fluxes of different flavours are probes of new physics entering the oscillation probability. For specificity we have used AGN sources, and calculated the changes induced in the well-known MPR bounds on both neutron-opaque and neutron-transparent sources. Our calculations can, in a straightforward manner, be repeated for other sources, or represented in terms of the WB bounds or in terms of actual fluxes and event rates.

We have discussed the Glashow Resonance process which is an important Standard Model process which should be considered in any interpretation of IceCube events seen in the energy range  $10^6 - 10^7$  GeV. It has a unique and background-free signature, the pure muon, which can be a smoking gun for this process. Besides the standard hadronic/electromagnetic cascade, the pure muon from  $\bar{\nu}_e e \rightarrow \bar{\nu}_\mu \mu$  and the contained lollipop signatures from  $\bar{\nu}_e e \rightarrow \bar{\nu}_\tau \tau$  were identified as clear signals of the resonance. Applying a Waxman-Bahcall  $E^{-2}$  flux in agreement with recent limits, the event numbers for general  $pp$  and  $p\gamma$  sources were evaluated. If the neutrino fluxes are positioned with such intensities as presently conjectured, the confirmation of the resonance is possible with several years of data collection at IceCube. The resonance could be used as a discovery tool for diffuse astrophysical neutrinos at PeV energies, and to obtain important information about cosmic-rays and astrophysical sources.

We have discussed the effects of several exotic, non-standard physics on the diffuse fluxes of the three neutrino flavours, using neutrino fluxes from standard extra-galactic sources such as AGN's. We have assumed a standard neutrino flux at source with the flavour ratio thereof being  $1 : 2 : 0$  and shown that due to standard oscillations in vacuum during the propagation of these neutrinos across cosmological distances the fluxes are evened out to the democratic value of  $1 : 1 : 1$ , and that even for non-standard fluxes at source the fluxes at the detector are still close to each other in magnitude and their spectral shapes are very similar.

Non-standard physics serves to destroy this equality among the three flavours and this serves as a potential probe for the underlying nature of the physics involved. To demonstrate this we first looked at how the decay of the heavier of the neutrinos affects the standard MPR diffuse flux bounds in the case of both normal and inverted hierarchies. We found that decay life-times of magnitudes several orders above those currently understood from experiment induce detectable changes in spectral shapes of the three diffuse fluxes, both against the standard flux, and among each other. Since the effects are strikingly different for the two hierarchies, it would also be possible to search for the hierarchy in case the heavier neutrinos do decay with life-times in the range  $10^{-3}$  s/eV  $- 10^4$  s/eV, as discussed here. We have also shown that the effects remain significant despite variation on the unknown parameters  $\theta_{13}$  and  $\delta_{CP}$  and probing neutrino decay within the life-times

explored here should be possible despite our limited knowledge about these parameters.

Tiny effects of Lorentz symmetry violation in the low energy theory arising due to the effect of some Planck scale physics can also be probed using ultra-high energy neutrinos. Taking the simplifying case of two neutrino flavours  $\nu_\mu$  and  $\nu_\tau$  we have described the effect of Lorentz violating parameters on transition probabilities between them during propagation and inferred that it leads to a strong decrease in the  $\nu_\tau$  flux as compared to the  $\nu_\mu$  flux. This breaks the  $\nu_\mu - \nu_\tau$  symmetry that is a feature of all standard model and most beyond standard-model scenarios, and thus provides us with a distinctive signature for LV. It translates to a corresponding decrease in the signature  $\nu_\tau$  events at high energies. While a simplifying case of two flavours and involving just the one Lorentz-violating parameter was dealt with here, the conclusions are true more generally. Detection of a sharp decrease in  $\tau$  events in future detectors like Auger and ANITA will be an indicator of the extent of Lorentz violation in low energies. Conversely, the failure to detect such a dip could be used to put bounds on the LV parameters.

Further, we have discussed the effect of decoherence and the existence of pseudo-Dirac neutrino states on the diffuse fluxes of the three flavours. While not as striking as the effects of neutrino decay or LV, the existence of pseudo-Dirac states affects distortions in the spectral shape of the standard flux at the lower end of the spectrum. On the contrary, decoherence shows almost no distortion on the fluxes. A probe of decoherence requires that we distinguish between neutrinos and anti-neutrinos since, irrespective of the flux ratio at source, it tries to bring the flux ratio to 1 : 1 : 1 at the detector, same as what standard oscillation does to the standard flux of 1 : 2 : 0. Even so, the effect of decoherence, seen at higher energies, is not significant and cannot, in all probability, be experimentally distinguished.

It is clear that future ultra-high energy neutrino detectors with strong flavour detection capabilities and excellent energy resolution will allow us to probe the validity of non-standard physical phenomena over large ranges of the involved parameters. While differences in spectra among the flavours arise due to the selectivity of non-standard physics with regard to the three families, strong distortion of spectral shape of the fluxes as compared to the standard flux expected at the detector arises due to the non-trivial energy dependence of transition probabilities in new physics. To detect or, potentially, constrain new physics it is necessary to carry out experiments that combine searches of both kinds. While understandably challenging, it will certainly be worthwhile carrying out detection experiments along these lines given the fundamental nature of physics that will be brought under the scanner.

# Bibliography

- [1] Y. Fukuda *et al.* [Super-Kamiokande Collaboration], Phys. Rev. Lett. **81**, 1158 (1998) [Erratum-ibid. **81**, 4279 (1998)] [hep-ex/9805021].
- [2] K. Hirata *et al.* [KAMIOKANDE-II Collaboration], Phys. Rev. Lett. **58**, 1490 (1987).
- [3] T. K. Gaisser and M. Honda, Ann. Rev. Nucl. Part. Sci. **52**, 153 (2002) [hep-ph/0203272].
- [4] K. Greisen, Phys. Rev. Lett. **16**, 748 (1966).
- [5] G. T. Zatsepin and V. A. Kuzmin, JETP Lett. **4**, 78 (1966) [Pisma Zh. Eksp. Teor. Fiz. **4**, 114 (1966)].
- [6] K. D. Hoffman, New J. Phys. **11**, 055006 (2009) [arXiv:0812.3809 [astro-ph]].
- [7] F. Halzen, J. Phys. Conf. Ser. **120**, 062004 (2008) [arXiv:0710.4158 [astro-ph]].
- [8] B. Baret [IceCube Collaboration], J. Phys. Conf. Ser. **110**, 062001 (2008).
- [9] F. Halzen, J. Phys. Conf. Ser. **171**, 012014 (2009) [J. Phys. Conf. Ser. **173**, 012021 (2009)] [arXiv:0901.4722 [astro-ph.HE]].
- [10] V. Aynutdinov, A. Avrorin, V. Balkanov, I. Belolaptikov, D. Bogorodsky, N. Budnev, I. Danilchenko and G. Domogatsky *et al.*, Nucl. Instrum. Meth. A **604**, S130 (2009).
- [11] A. Margiotta [ANTARES Collaboration], Nucl. Phys. Proc. Suppl. **190**, 121 (2009).
- [12] D. Z. Besson, J. Phys. Conf. Ser. **81**, 012008 (2007).
- [13] P. W. Gorham, P. Allison, S. W. Barwick, J. J. Beatty, D. Z. Besson, W. R. Binns, C. Chen and P. Chen *et al.*, J. Phys. Conf. Ser. **136**, 022052 (2008).
- [14] A. P. Roth,
- [15] R. U. Abbasi *et al.* [HiRes Collaboration], Phys. Rev. Lett. **100**, 101101 (2008) [astro-ph/0703099].
- [16] J. G. Learned and S. Pakvasa, Astropart. Phys. **3**, 267 (1995) [hep-ph/9405296, hep-ph/9408296].
- [17] H. Athar, M. Jezabek and O. Yasuda, Phys. Rev. D **62**, 103007 (2000) [hep-ph/0005104].
- [18] M. C. Gonzalez-Garcia, M. Maltoni and J. Salvado, JHEP **1004**, 056 (2010) [arXiv:1001.4524 [hep-ph]].

- [19] A. Bandyopadhyay, S. Choubey, S. Goswami, S. T. Petcov and D. P. Roy, arXiv:0804.4857 [hep-ph].
- [20] G. L. Fogli, E. Lisi, A. Marrone, A. Palazzo and A. M. Rotunno, Phys. Rev. Lett. **101**, 141801 (2008) [arXiv:0806.2649 [hep-ph]].
- [21] A. Bhattacharya, S. Choubey, R. Gandhi and A. Watanabe, Phys. Lett. B **690**, 42 (2010) [arXiv:0910.4396 [hep-ph]].
- [22] T. Kashti and E. Waxman, Phys. Rev. Lett. **95**, 181101 (2005) [astro-ph/0507599].
- [23] B. Baret [IceCube Collaboration], J. Phys. Conf. Ser. **110**, 062001 (2008).
- [24] K. Mannheim, R. J. Protheroe and J. P. Rachen, Phys. Rev. D **63**, 023003 (2001) [astro-ph/9812398].
- [25] M. Maltoni and T. Schwetz, PoS IDM **2008**, 072 (2008) [arXiv:0812.3161 [hep-ph]].
- [26] E. Waxman and J. N. Bahcall, Phys. Rev. D **59**, 023002 (1999) [hep-ph/9807282].
- [27] J. G. Learned and S. Pakvasa, Astropart. Phys. **3**, 267 (1995) [hep-ph/9405296, hep-ph/9408296].
- [28] H. Athar, M. Jezabek and O. Yasuda, Phys. Rev. D **62**, 103007 (2000) [hep-ph/0005104].
- [29] M. C. Gonzalez-Garcia, M. Maltoni and J. Salvado, JHEP **1004**, 056 (2010) [arXiv:1001.4524 [hep-ph]].
- [30] A. Bandyopadhyay, S. Choubey, S. Goswami, S. T. Petcov and D. P. Roy, arXiv:0804.4857 [hep-ph].
- [31] G. L. Fogli, E. Lisi, A. Marrone, A. Palazzo and A. M. Rotunno, Phys. Rev. Lett. **101**, 141801 (2008) [arXiv:0806.2649 [hep-ph]].
- [32] T. Kashti and E. Waxman, Phys. Rev. Lett. **95**, 181101 (2005) [astro-ph/0507599].
- [33] J. F. Beacom, N. F. Bell, D. Hooper, S. Pakvasa and T. J. Weiler, Phys. Rev. Lett. **90**, 181301 (2003) [hep-ph/0211305].
- [34] J. F. Beacom, N. F. Bell, D. Hooper, S. Pakvasa and T. J. Weiler, Phys. Rev. D **68**, 093005 (2003) [Erratum-ibid. D **72**, 019901 (2005)] [hep-ph/0307025].
- [35] G. Barenboim and C. Quigg, Phys. Rev. D **67**, 073024 (2003) [hep-ph/0301220].
- [36] P. Keranen, J. Maalampi, M. Myrskylainen and J. Riittinen, Phys. Lett. B **574**, 162 (2003) [hep-ph/0307041].

- [37] J. F. Beacom, N. F. Bell, D. Hooper, J. G. Learned, S. Pakvasa and T. J. Weiler, Phys. Rev. Lett. **92**, 011101 (2004) [hep-ph/0307151].
- [38] D. Hooper, D. Morgan and E. Winstanley, Phys. Lett. B **609**, 206 (2005) [hep-ph/0410094].
- [39] D. Hooper, D. Morgan and E. Winstanley, Phys. Rev. D **72**, 065009 (2005) [hep-ph/0506091].
- [40] D. Meloni and T. Ohlsson, Phys. Rev. D **75**, 125017 (2007) [hep-ph/0612279].
- [41] Z. -z. Xing and S. Zhou, Phys. Lett. B **666**, 166 (2008) [arXiv:0804.3512 [hep-ph]].
- [42] A. Esmaili and Y. Farzan, Nucl. Phys. B **821**, 197 (2009) [arXiv:0905.0259 [hep-ph]].
- [43] Y. Farzan and A. Y. Smirnov, Phys. Rev. D **65**, 113001 (2002) [hep-ph/0201105].
- [44] J. F. Beacom, N. F. Bell, D. Hooper, S. Pakvasa and T. J. Weiler, Phys. Rev. D **69**, 017303 (2004) [hep-ph/0309267].
- [45] P. D. Serpico and M. Kachelriess, Phys. Rev. Lett. **94**, 211102 (2005) [hep-ph/0502088].
- [46] Z. -z. Xing, Phys. Rev. D **74**, 013009 (2006) [hep-ph/0605219].
- [47] W. Rodejohann, JCAP **0701**, 029 (2007) [hep-ph/0612047].
- [48] W. Winter, Phys. Rev. D **74**, 033015 (2006) [hep-ph/0604191].
- [49] R. L. Awasthi and S. Choubey, Phys. Rev. D **76**, 113002 (2007) [arXiv:0706.0399 [hep-ph]].
- [50] P. Lipari, M. Lusignoli and D. Meloni, Phys. Rev. D **75**, 123005 (2007) [arXiv:0704.0718 [astro-ph]].
- [51] K. Blum, Y. Nir and E. Waxman, arXiv:0706.2070 [hep-ph].
- [52] S. Pakvasa, W. Rodejohann and T. J. Weiler, JHEP **0802**, 005 (2008) [arXiv:0711.4517 [hep-ph]].
- [53] S. Choubey, V. Niro and W. Rodejohann, Phys. Rev. D **77**, 113006 (2008) [arXiv:0803.0423 [hep-ph]].
- [54] E. Waxman and J. N. Bahcall, Phys. Rev. D **59**, 023002 (1999) [hep-ph/9807282].
- [55] K. Mannheim, R. J. Protheroe and J. P. Rachen, Phys. Rev. D **63**, 023003 (2001) [astro-ph/9812398].

- [56] M. Maltoni and T. Schwetz, PoS IDM **2008**, 072 (2008) [arXiv:0812.3161 [hep-ph]].
- [57] J. G. Learned and S. Pakvasa, Astropart. Phys. **3**, 267 (1995) [hep-ph/9405296, hep-ph/9408296].
- [58] H. Athar, M. Jezabek and O. Yasuda, Phys. Rev. D **62**, 103007 (2000) [hep-ph/0005104].
- [59] M. C. Gonzalez-Garcia, M. Maltoni and J. Salvado, JHEP **1004**, 056 (2010) [arXiv:1001.4524 [hep-ph]].
- [60] A. Bandyopadhyay, S. Choubey, S. Goswami, S. T. Petcov and D. P. Roy, arXiv:0804.4857 [hep-ph].
- [61] G. L. Fogli, E. Lisi, A. Marrone, A. Palazzo and A. M. Rotunno, Phys. Rev. Lett. **101**, 141801 (2008) [arXiv:0806.2649 [hep-ph]].
- [62] A. Bhattacharya, S. Choubey, R. Gandhi and A. Watanabe, Phys. Lett. B **690**, 42 (2010) [arXiv:0910.4396 [hep-ph]].
- [63] T. Kashti and E. Waxman, Phys. Rev. Lett. **95**, 181101 (2005) [astro-ph/0507599].
- [64] J. F. Beacom, N. F. Bell, D. Hooper, S. Pakvasa and T. J. Weiler, Phys. Rev. Lett. **90**, 181301 (2003) [hep-ph/0211305].
- [65] J. F. Beacom, N. F. Bell, D. Hooper, S. Pakvasa and T. J. Weiler, Phys. Rev. D **68**, 093005 (2003) [Erratum-ibid. D **72**, 019901 (2005)] [hep-ph/0307025].
- [66] G. Barenboim and C. Quigg, Phys. Rev. D **67**, 073024 (2003) [hep-ph/0301220].
- [67] P. Keranen, J. Maalampi, M. Myyrylainen and J. Riittinen, Phys. Lett. B **574**, 162 (2003) [hep-ph/0307041].
- [68] J. F. Beacom, N. F. Bell, D. Hooper, J. G. Learned, S. Pakvasa and T. J. Weiler, Phys. Rev. Lett. **92**, 011101 (2004) [hep-ph/0307151].
- [69] D. Hooper, D. Morgan and E. Winstanley, Phys. Lett. B **609**, 206 (2005) [hep-ph/0410094].
- [70] D. Hooper, D. Morgan and E. Winstanley, Phys. Rev. D **72**, 065009 (2005) [hep-ph/0506091].
- [71] D. Meloni and T. Ohlsson, Phys. Rev. D **75**, 125017 (2007) [hep-ph/0612279].
- [72] Z. -z. Xing and S. Zhou, Phys. Lett. B **666**, 166 (2008) [arXiv:0804.3512 [hep-ph]].
- [73] A. Esmaili and Y. Farzan, Nucl. Phys. B **821**, 197 (2009) [arXiv:0905.0259 [hep-ph]].

- [74] Y. Farzan and A. Y. Smirnov, Phys. Rev. D **65**, 113001 (2002) [hep-ph/0201105].
- [75] J. F. Beacom, N. F. Bell, D. Hooper, S. Pakvasa and T. J. Weiler, Phys. Rev. D **69**, 017303 (2004) [hep-ph/0309267].
- [76] P. D. Serpico and M. Kachelriess, Phys. Rev. Lett. **94**, 211102 (2005) [hep-ph/0502088].
- [77] Z. -z. Xing, Phys. Rev. D **74**, 013009 (2006) [hep-ph/0605219].
- [78] W. Rodejohann, JCAP **0701**, 029 (2007) [hep-ph/0612047].
- [79] W. Winter, Phys. Rev. D **74**, 033015 (2006) [hep-ph/0604191].
- [80] R. L. Awasthi and S. Choubey, Phys. Rev. D **76**, 113002 (2007) [arXiv:0706.0399 [hep-ph]].
- [81] P. Lipari, M. Lusignoli and D. Meloni, Phys. Rev. D **75**, 123005 (2007) [arXiv:0704.0718 [astro-ph]].
- [82] K. Blum, Y. Nir and E. Waxman, arXiv:0706.2070 [hep-ph].
- [83] S. Pakvasa, W. Rodejohann and T. J. Weiler, JHEP **0802**, 005 (2008) [arXiv:0711.4517 [hep-ph]].
- [84] S. Choubey, V. Niro and W. Rodejohann, Phys. Rev. D **77**, 113006 (2008) [arXiv:0803.0423 [hep-ph]].
- [85] E. Waxman and J. N. Bahcall, Phys. Rev. D **59**, 023002 (1999) [hep-ph/9807282].
- [86] K. Mannheim, R. J. Protheroe and J. P. Rachen, Phys. Rev. D **63**, 023003 (2001) [astro-ph/9812398].
- [87] M. Maltoni and T. Schwetz, PoS IDM **2008**, 072 (2008) [arXiv:0812.3161 [hep-ph]].
- [88] J. F. Beacom and N. F. Bell, Phys. Rev. D **65**, 113009 (2002) [hep-ph/0204111].
- [89] D. E. Groom *et al.* [Particle Data Group Collaboration], Eur. Phys. J. C **15**, 1 (2000).
- [90] S. Pakvasa, AIP Conf. Proc. **542**, 99 (2000) [hep-ph/0004077].
- [91] M. S. Bilenky and A. Santamaria, Phys. Lett. B **336**, 91 (1994) [hep-ph/9405427].
- [92] P. W. Gorham *et al.* [ANITA Collaboration], Phys. Rev. Lett. **103**, 051103 (2009) [arXiv:0812.2715 [astro-ph]].
- [93] P. D. Serpico, Phys. Rev. Lett. **98**, 171301 (2007) [astro-ph/0701699].

- [94] A. Friedland, K. M. Zurek and S. Bashinsky, arXiv:0704.3271 [astro-ph].
- [95] R. M. Bionta, G. Blewitt, C. B. Bratton, D. Casper, A. Ciocio, R. Claus, B. Cortez and M. Crouch *et al.*, Phys. Rev. Lett. **58**, 1494 (1987).
- [96] K. Hirata *et al.* [KAMIOKANDE-II Collaboration], Phys. Rev. Lett. **58**, 1490 (1987).
- [97] D. F. Cowen [IceCube Collaboration], J. Phys. Conf. Ser. **60**, 227 (2007).
- [98] J. L. Feng, P. Fisher, F. Wilczek and T. M. Yu, Phys. Rev. Lett. **88**, 161102 (2002) [hep-ph/0105067].
- [99] R. Gandhi, C. Quigg, M. H. Reno and I. Sarcevic, Astropart. Phys. **5**, 81 (1996) [hep-ph/9512364].
- [100] R. Gandhi, C. Quigg, M. H. Reno and I. Sarcevic, Phys. Rev. D **58**, 093009 (1998) [hep-ph/9807264].
- [101] M. Apollonio *et al.* [CHOOZ Collaboration], Eur. Phys. J. C **27**, 331 (2003) [hep-ex/0301017].
- [102] J. Madore, S. Schraml, P. Schupp and J. Wess, Eur. Phys. J. C **16**, 161 (2000) [hep-th/0001203].
- [103] V. A. Kostelecky, Phys. Rev. D **69**, 105009 (2004) [hep-th/0312310].
- [104] O. W. Greenberg, Phys. Rev. Lett. **89**, 231602 (2002) [hep-ph/0201258].
- [105] C. Rovelli and L. Smolin, Nucl. Phys. B **442**, 593 (1995) [Erratum-ibid. B **456**, 753 (1995)] [gr-qc/9411005].
- [106] R. Gambini and J. Pullin, Phys. Rev. D **59**, 124021 (1999) [gr-qc/9809038].
- [107] J. Alfaro, H. A. Morales-Tecotl and L. F. Urrutia, Phys. Rev. Lett. **84**, 2318 (2000) [gr-qc/9909079].
- [108] G. Amelino-Camelia, L. Smolin and A. Starodubtsev, Class. Quant. Grav. **21**, 3095 (2004) [hep-th/0306134].
- [109] L. Freidel, J. Kowalski-Glikman and L. Smolin, Phys. Rev. D **69**, 044001 (2004) [hep-th/0307085].
- [110] V. A. Kostelecky and M. Mewes, Phys. Rev. D **69**, 016005 (2004) [hep-ph/0309025].
- [111] S. Hannestad and G. Raffelt, Phys. Rev. D **72**, 103514 (2005) [hep-ph/0509278].
- [112] T. Thiemann, Cambridge, UK: Cambridge Univ. Pr. (2007) 819 p [gr-qc/0110034].

- [113] J. Abraham *et al.* [Pierre Auger Collaboration], Phys. Rev. D **79**, 102001 (2009) [arXiv:0903.3385 [astro-ph.HE]].
- [114] N. F. Bell, E. Pierpaoli and K. Sigurdson, Phys. Rev. D **73**, 063523 (2006) [astro-ph/0511410].
- [115] M. Maltoni and W. Winter, JHEP **0807**, 064 (2008) [arXiv:0803.2050 [hep-ph]].
- [116] L. A. Anchordoqui, H. Goldberg, M. C. Gonzalez-Garcia, F. Halzen, D. Hooper, S. Sarkar and T. J. Weiler, Phys. Rev. D **72**, 065019 (2005) [hep-ph/0506168].
- [117] J. Abraham *et al.* [Pierre Auger Collaboration], Phys. Lett. B **685**, 239 (2010) [arXiv:1002.1975 [astro-ph.HE]].
- [118] A. Esmaili, Phys. Rev. D **81**, 013006 (2010) [arXiv:0909.5410 [hep-ph]].
- [119] B. Baret [IceCube Collaboration], J. Phys. Conf. Ser. **110** (2008) 062001.
- [120] F. Halzen, J. Phys. Conf. Ser. **171** (2009) 012014.
- [121] V. Aynutdinov, A. Avrorin, V. Balkanov, I. Belolaptikov, D. Bogorodsky, N. Budnev, I. Danilchenko, G. Domogatsky *et al.*, Nucl. Instrum. Meth. **A602** (2009) 14-20.
- [122] A. Margiotta [ANTARES Collaboration], Nucl. Phys. Proc. Suppl. **190** (2009) 121-126; J. A. Aguilar *et al.* [ANTARES Collaboration], Phys. Lett. **B696** (2011) 16-22.
- [123] D. Z. Besson, J. Phys. Conf. Ser. **81** (2007) 012008; I. Kravchenko, D. Seckel, D. Besson, J. Ralston, J. Taylor, K. Ratzlaff, R. Young, arXiv:1106.1164.
- [124] P. W. Gorham, P. Allison, S. W. Barwick, J. J. Beatty, D. Z. Besson, W. R. Binns, C. Chen, P. Chen *et al.*, J. Phys. Conf. Ser. **136** (2008) 022052; P. W. Gorham *et al.* [The ANITA Collaboration], Phys. Rev. **D82** (2010) 022004.
- [125] A. Margiotta [KM3NeT Collaboration], J. Phys. Conf. Ser. **203** (2010) 012124.
- [126] See *e.g.*, H. Athar, M. Jezabek, O. Yasuda, Phys. Rev. **D62** (2000) 103007; G. Barenboim, C. Quigg, Phys. Rev. **D67** (2003) 073024; J. F. Beacom, N. F. Bell, D. Hooper, S. Pakvasa, T. J. Weiler, Phys. Rev. **D68** (2003) 093005; P. D. Serpico, M. Kachelriess, Phys. Rev. Lett. **94** (2005) 211102; Z. -z. Xing, Phys. Rev. **D74** (2006) 013009; W. Rodejohann, JCAP **0701** (2007) 029; P. Lipari, M. Lusignoli, D. Meloni, Phys. Rev. **D75** (2007) 123005; K. Blum, Y. Nir, E. Waxman, arXiv:0706.2070; S. Pakvasa, W. Rodejohann, T. J. Weiler, JHEP **0802** (2008) 005; A. Esmaili, Y. Farzan, Nucl. Phys. **B821** (2009) 197-214; S. Choubey, W. Rodejohann, Phys. Rev. **D80**, 113006 (2009).
- [127] S. Pakvasa, Mod. Phys. Lett. **A23** (2008) 1313-1324.

- [128] J. F. Beacom, N. F. Bell, D. Hooper, S. Pakvasa, T. J. Weiler, Phys. Rev. Lett. **90** (2003) 181301; Phys. Rev. **D69** (2004) 017303; M. Maltoni, W. Winter, JHEP **0807** (2008) 064.
- [129] J. F. Beacom, N. F. Bell, D. Hooper, J. G. Learned, S. Pakvasa, T. J. Weiler, Phys. Rev. Lett. **92** (2004) 011101; P. Keranen, J. Maalampi, M. Myyrylainen, J. Riittinen, Phys. Lett. **B574** (2003) 162-168; A. Esmaili, Phys. Rev. **D81** (2010) 013006; J. Barry, R. N. Mohapatra, W. Rodejohann, Phys. Rev. **D83** (2011) 113012.
- [130] D. Hooper, D. Morgan, E. Winstanley, Phys. Rev. **D72** (2005) 065009.
- [131] A. Bhattacharya, S. Choubey, R. Gandhi, A. Watanabe, Phys. Lett. **B690** (2010) 42-47; JCAP **1009** (2010) 009.
- [132] S. L. Glashow, Phys. Rev. **118** (1960) 316-317.
- [133] V. S. Berezinsky, A. Z. Gazizov, JETP Lett. **25**, 254-256 (1977).
- [134] V. S. Berezinsky, A. Z. Gazizov, Sov. J. Nucl. Phys. **33**, 120-125 (1981).
- [135] L. A. Anchordoqui, H. Goldberg, F. Halzen, T. J. Weiler, Phys. Lett. **B621** (2005) 18-21.
- [136] P. Bhattacharjee, N. Gupta, hep-ph/0501191.
- [137] S. Hummer, M. Maltoni, W. Winter, C. Yaguna, Astropart. Phys. **34** (2010) 205-224; P. Mehta, W. Winter, JCAP **1103** (2011) 041.
- [138] Z. -z. Xing, S. Zhou, arXiv:1105.4114 [hep-ph].
- [139] E. Waxman, J. N. Bahcall, Phys. Rev. **D59** (1999) 023002.
- [140] R. Abbasi *et al.* [IceCube Collaboration], Phys. Rev. **D83** (2011) 092003; arXiv:1104.5187.
- [141] R. Gandhi, C. Quigg, M. H. Reno and I. Sarcevic, Astropart. Phys. **5**, 81 (1996); Phys. Rev. D **58**, 093009 (1998).
- [142] J. G. Learned, S. Pakvasa, Astropart. Phys. **3** (1995) 267-274.
- [143] A. Bhattacharya, R. Gandhi, W. Rodejohann, A. Watanabe, in preparation.
- [144] G. J. Feldman, R. D. Cousins, Phys. Rev. **D57** (1998) 3873-3889.